Author/s:
Wragg, KM;Tan, HX;Kristensen, AB;Nguyen-Robertson, CV;Kelleher, AD;Parsons, MS;Wheatley, AK;Berzins, SP;Pellicci, DG;Kent, SJ;Juno, JA

Title:
High CD26 and Low CD94 Expression Identifies an IL-23 Responsive Vδ2+ T Cell Subset with a MAIT Cell-like Transcriptional Profile

Date:
2020-06-16

Citation:
Wragg, K. M., Tan, H. X., Kristensen, A. B., Nguyen-Robertson, C. V., Kelleher, A. D., Parsons, M. S., Wheatley, A. K., Berzins, S. P., Pellicci, D. G., Kent, S. J. & Juno, J. A. (2020). High CD26 and Low CD94 Expression Identifies an IL-23 Responsive Vδ2+ T Cell Subset with a MAIT Cell-like Transcriptional Profile. Cell Reports, 31 (11), https://doi.org/10.1016/j.celrep.2020.107773.

Persistent Link:
https://hdl.handle.net/11343/252446

Cell Reports

Article

High CD26 and Low CD94 Expression Identifies an IL-23 Responsive Vδ2^{+} T Cell Subset with a MAIT Cell-like Transcriptional Profile

Graphical Abstract

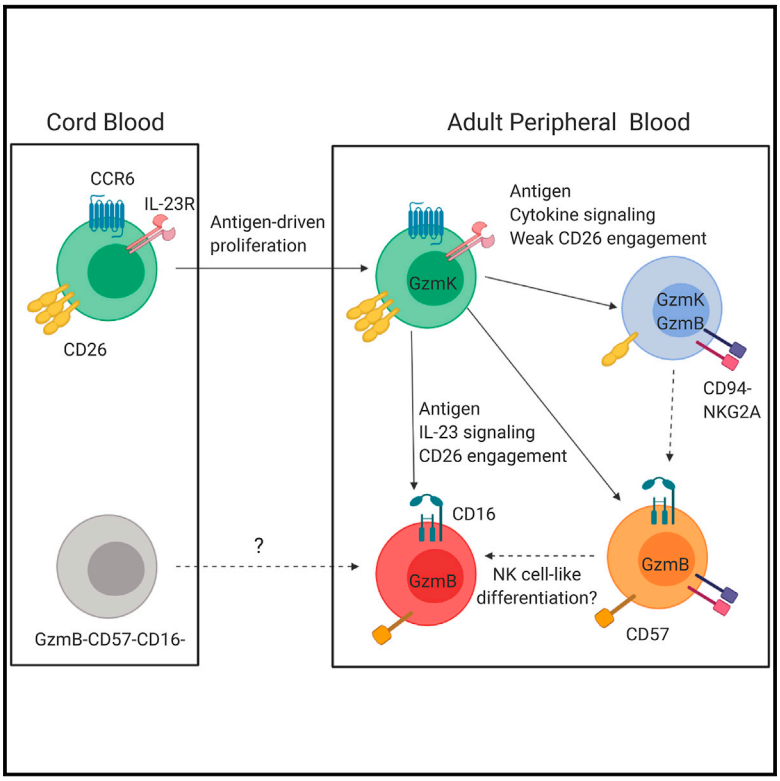

Highlights

- Human CD26^{hi}CD94^{lo} Vd2Vg9 T cells exhibit a MAIT cell-like phenotype
- CD26 and CD94 regulate Vd2 cytokine responses and cytotoxicity
- Cord blood Vd2Vg9 cells are predominately CD26^{hi}CD94^{lo}
- Exposure of CD26^{hi}CD94^{lo} cells to antigen and IL-23 induces a cytotoxic phenotype

Authors

Kathleen M. Wragg, Hyon-Xhi Tan, Anne B. Kristensen, ..., Daniel G. Pellicci, Stephen J. Kent, Jennifer A. Juno

Correspondence

skent@unimelb.edu.au (S.J.K.), jennifer.juno@unimelb.edu.au (J.A.J.)

In Brief

Wragg et al. identify a population of human gd T cells with striking similarities to MAIT cells. These cells dominate the cord blood Vd2 population and upregulate an effector-like program upon antigen and IL-23 stimulation, providing a potential mechanism by which cytotoxic Vd2 cells may accumulate during adolescence and adulthood.

Wragg et al., 2020, Cell Reports *31*, 107773
June 16, 2020
https://doi.org/10.1016/j.celrep.2020.107773

CellPress

Cell Reports

CellPress
OPEN ACCESS

Article

High CD26 and Low CD94 Expression Identifies an IL-23 Responsive Vδ2$^+$ T Cell Subset with a MAIT Cell-like Transcriptional Profile

Kathleen M. Wragg,[1] Hyon-Xhi Tan,[1] Anne B. Kristensen,[1] Catriona V. Nguyen-Robertson,[1,2] Anthony D. Kelleher,[3,4] Matthew S. Parsons,[1,5,6] Adam K. Wheatley,[1] Stuart P. Berzins,[1,7] Daniel G. Pellicci,[1,8] Stephen J. Kent,[1,9,10,*] and Jennifer A. Juno[1,11,*]

[1]Department of Microbiology and Immunology, Peter Doherty Institute for Infection and Immunity, University of Melbourne, Melbourne, VIC 3000, Australia
[2]ARC Centre of Excellence in Advanced Molecular Imaging, University of Melbourne, Melbourne, VIC 3000, Australia
[3]The Kirby Institute, University of New South Wales, Kensington, NSW 2052, Australia
[4]St. Vincent's Centre for Applied Medical Research, St. Vincent's Hospital, Darlinghurst, NSW 2011, Australia
[5]Division of Microbiology and Immunology, Yerkes National Primate Research Center, Atlanta, GA 30329, USA
[6]Department of Pathology and Laboratory Medicine, School of Medicine, Emory University, Atlanta, GA 30322, USA
[7]Federation University and Fiona Elsey Cancer Research Institute, Ballarat, VIC 3350, Australia
[8]Murdoch Children's Research Institute, Parkville, VIC 3052, Australia
[9]Melbourne Sexual Health Centre and Department of Infectious Diseases, Alfred Health, Central Clinical School, Monash University, Carlton, VIC 3053, Australia
[10]ARC Centre of Excellence in Convergent Bio-Nano Science and Technology, University of Melbourne, Melbourne, VIC 3000, Australia
[11]Lead Contact
*Correspondence: skent@unimelb.edu.au (S.J.K.), jennifer.juno@unimelb.edu.au (J.A.J.)
https://doi.org/10.1016/j.celrep.2020.107773

SUMMARY

Vδ2$^+$ T cells play a critical role in immunity to micro-organisms and cancer but exhibit substantial heterogeneity in humans. Here, we demonstrate that CD26 and CD94 define transcriptionally, phenotypically, and functionally distinct Vδ2$^+$ T cell subsets. Despite distinct antigen specificities, CD26^{hi}CD94^{lo} Vδ2$^+$ cells exhibit substantial similarities to CD26^{hi} mucosal-associated invariant T (MAIT) cells, although CD26$^-$ Vδ2$^+$ cells exhibit cytotoxic, effector-like profiles. At birth, the Vδ2$^+$Vγ9$^+$ population is dominated by CD26^{hi}CD94^{lo} cells; during adolescence and adulthood, Vδ2$^+$ cells acquire CD94/NKG2A expression and the relative frequency of the CD26^{hi}CD94^{lo} subset declines. Critically, exposure of the CD26^{hi}CD94^{lo} subset to phosphoantigen in the context of interleukin-23 (IL-23) and CD26 engagement drives the acquisition of a cytotoxic program and concurrent loss of the MAIT cell-like phenotype. The ability to modulate the cytotoxic potential of CD26^{hi}CD94^{lo} Vδ2$^+$ cells, combined with their adenosine-binding capacity, may make them ideal targets for immunotherapeutic expansion and adoptive transfer.

INTRODUCTION

Gamma delta (γδ) T cells are a diverse subset of unconventional T cells that recognize non-peptide antigens presented by molecules other than classical major histocompatibility complex (MHC) proteins (Godfrey et al., 2015). Vδ2 T cell receptor (TCR)-expressing cells are the most abundant γδ T cell subset in human peripheral blood, due in large part to polyclonal expansion of Vδ2$^+$Vγ9$^+$ cells that recognize phosphoantigens (Harly et al., 2012). Vδ2$^+$ T cells are involved in immunity to a variety of infections, including *Mycobacterium tuberculosis* (Qaqish et al., 2017), *Plasmodium spp* (Jagannathan et al., 2017), and HIV-1 (Li et al., 2013; Juno and Eriksson, 2019), as well as immune surveillance against tumors (Lawand et al., 2017).

Many unconventional T cells share common characteristics, including a blend of T cell and natural killer (NK) cell transcriptional programming that endows them with innate-like functions. In addition to expression of the transcription factor PLZF, iNKT cells, MAIT cells, and Vδ2$^+$ T cells commonly express surface markers, such as CD161, interleukin-18Rα (IL-18Rα), CCR6, and CCR5. Despite similarities in MAIT and Vδ2$^+$ T cell phenotype, however, Vδ2$^+$ T cells also exhibit effector-like populations expressing CD16, CX3CR1, CD57, and GzmB, none of which are typical of MAIT cells (Provine et al., 2018; Ryan et al., 2016). CD161 is proposed as a marker to identify cytokine-responsive Vδ2$^+$ T cells (Provine et al., 2018; Fergusson et al., 2014), but a substantial proportion of CD161$^-$ Vδ2$^+$ T cells respond to cytokine stimulation (Provine et al., 2018), although CD161$^+$ Vδ1$^+$ T cells do not respond to cytokine stimulation (Provine et al., 2018), suggesting that the relationship between CD161 expression and cytokine responsiveness among γδ T cells is not absolute.

Characterization of fetal and cord blood Vδ2$^+$Vγ9$^+$ cells suggests that GzmB$^-$IL-18Rα$^+$ cells predominate at birth and that cytotoxicity is acquired post-natally (Dimova et al., 2015). Many questions remain, however, regarding the mechanisms regulating the formation of cytotoxic Vδ2$^+$ T cells, as their frequency is unrelated to immune senescence or phosphoantigen exposure (Ryan et al., 2016). Studies have shown enrichment of CCR6 and IL-18Rα expression within the CD28$^+$CD27$^+$ CD45RO$^+$ Vδ2$^+$ T cell subset (Ryan et al., 2016), but it is unclear how these subsets relate to the expression of CD161 or transcriptional profiles associated with other PLZF$^+$ unconventional T cells. A better understanding of Vδ2$^+$ T cell heterogeneity and differentiation will have important implications for the use of these cells in γδ T-cell-based immunotherapy, which to date has exhibited sub-optimal efficacy in many patients (Hoeres et al., 2018; Zhao et al., 2018; Pauza et al., 2018).

In addition to CD161, MAIT cells almost uniformly express high levels of CD26 (Sharma et al., 2015; Gherardin et al., 2018; Dusseaux et al., 2011), a protein we previously found to correlate with γδ T cell cytokine responsiveness (Juno et al., 2017). CD26 binds caveolin-1 (Ohnuma et al., 2004, 2007) to provide co-stimulatory signals in combination with CD3/TCR triggering (Dang et al., 1990; Hatano et al., 2014) and serves as a membrane anchor for adenosine deaminase (ADA) (Kameoka et al., 1993). Other markers associated with MAIT cell cytokine responsiveness include CD56 and CD94 (Dias et al., 2017). Notably, CD94 is also associated with cytokine responsiveness by NK cells (Yu et al., 2010) and can regulate T cell and NK cell function via co-expression with the inhibitory receptor NKG2A or the activating receptor NKG2C (Lazetic et al., 1996).

In this study, we find that human CD26 and CD94 expression patterns identify transcriptionally distinct Vδ2$^+$ T cell subsets that differ in the expression of key transcriptional regulators and define functional subsets independently of classical memory markers. In particular, CD26^{hi}CD94^{lo} Vδ2$^+$ T cells exhibit strong transcriptional, phenotypic, and functional similarities to MAIT cells. Analysis of cord blood samples confirms that CD26^{hi}CD94^{lo} Vδ2$^+$ T cells predominate at birth, and we find evidence that the combination of antigen, IL-23 exposure, and CD26 ligation can contribute to the generation of CD26$^-$ cytotoxic Vδ2$^+$ T cells in adults.

RESULTS

Expression of CD26 and CD94 Describes Stable Phenotypes Related to Vδ2$^+$ T Cell Frequency

Given reports of CD26 and CD94 expression on MAIT cells, we investigated the expression of these markers on Vδ2$^+$ T cells. CD26 is expressed at varying density on Vδ2$^+$ T cells *ex vivo*, allowing for discrimination of CD26^{hi}, CD26$^+$, and CD26$^-$ cells (Figure 1A). Similarly, CD94 is expressed on a substantial proportion of Vδ2$^+$ cells in either a CD94^{hi} or CD94^{lo} population (Figure 1A). Strikingly, the proportion of total CD26$^{hi/+}$ Vδ2$^+$ T cells was highest in donors with low Vδ2$^+$ T cell frequencies (<5% of bulk T cells) and exhibited an inverse correlation with total Vδ2$^+$ T cell frequency (Figure 1B; p = 0.0016). CD26 and CD94 co-expression consistently demarcated four populations of Vδ2$^+$ T cells (Figure 1C), with CD26 median fluorescence intensity (MFI) being significantly higher among CD26$^{hi/+}$CD94^{lo} cells relative to CD26$^{hi/+}$CD94$^+$ cells (Figure 1C; p = 0.008). Despite a minor enrichment of CD161 expression on CD26^{hi}CD94^{lo} cells, CD161 was highly expressed on all four CD26/CD94 Vδ2$^+$ T cell subsets, even in donors with substantial frequencies of CD26$^-$ Vδ2$^+$ T cells (Figures 1D and 1E).

Consistent with the reported heterogeneity of Vδ2$^+$ T cells (Angelini et al., 2004; Bank and Marcu-Malina, 2014), the *ex vivo* frequency of each CD26/CD94 subset varied across 23 human donors (Figure S1A), although the CD26$^+$CD94^{hi} subset tended to predominate (Figure 1F). An individual's Vδ2$^+$ T cell phenotype was maintained over repeat sampling, regardless of the distribution of CD26/CD94 co-expression (Figure S1B). We confirmed that CD26/CD94 subsets are a feature of Vδ2$^+$Vγ9$^+$ phosphoantigen-reactive T cells and not the recently described Vδ2$^+$Vγ9$^-$ T cell subset (Figures S1C and S1D), which is consistent with reports that the Vδ2 TCR-specific B6 antibody used in this study preferentially identifies Vδ2$^+$Vγ9$^+$ cells (Davey et al., 2018).

CD26/CD94 Expression Defines Vδ2$^+$ T Cell Subsets with Distinct RNA Transcriptomes

To determine whether CD26/CD94 subpopulations represented transcriptionally distinct Vδ2$^+$ T cell subsets, CD26$^{hi/+}$CD94^{lo}, CD26$^{hi/+}$CD94^{hi}, CD26$^-$CD94^{hi}, and CD26$^-$CD94^{lo} cells were sorted from three healthy donors and subjected to RNA sequencing. Clustering of the samples based on the expression of 298 differentially regulated genes (DRGs) (false discovery rate [FDR] < 0.05; absolute fold change [FC] > 1.5; Table S1) clearly discriminated the four CD26/CD94 populations (Figures 2A and 2B). Hierarchical clustering of the top 50 up- and downregulated transcripts (based on the fold change of the CD26$^{hi/+}$CD94^{lo} population compared to the average) highlighted the substantial differences between CD26$^{hi/+}$CD94^{lo} cells and both CD26$^-$ subsets, with the CD26$^{hi/+}$CD94^{hi} cells presenting an intermediary signature (Figure 2C).

Expression of a number of transcription factors varied significantly across the subsets (Figure 2D), including RORc, Zeb2 (a regulator of NK cell cytotoxicity; van Helden et al., 2015), and the master regulator Tbet (Figure 2E). Hobit was also detected but fell above the FDR cutoff (FDR = 0.09; Figure 2E). Interestingly, there were no differences in the expression of PLZF (Figure 2E). Both CD26$^+$ Vδ2$^+$ T cell subsets were enriched for expression of multiple chemokine receptors (CCR5, CCR2, CCR1, and CCR6), cytokine receptors (IL-23R), and interferon (IFN)-related genes (IFNG-AS1), although the two CD26$^-$ Vδ2$^+$ T cell populations were enriched for cytotoxicity-related transcripts, including CD16, GzmB, CX3CR1, perforin, and CD57 (B3GAT1; Figures 2F and 2G).

CD26$^+$CD94^{lo} Vδ2$^+$ Cells Are Transcriptionally Similar to MAIT Cells

A striking feature of the RNA sequencing (RNA-seq) dataset was the co-expression of RORc, CCR6, IL-23R, and GzmK RNA, combined with a lack of GzmB expression, in the CD26$^{hi/+}$ CD94^{lo} subset. These features, in addition to PLZF and IL-18Rα expression, are highly characteristic of MAIT cells (Dusseaux et al., 2011; Kurioka et al., 2015). We therefore incorporated a published human MAIT cell transcriptome (Hinks et al.,

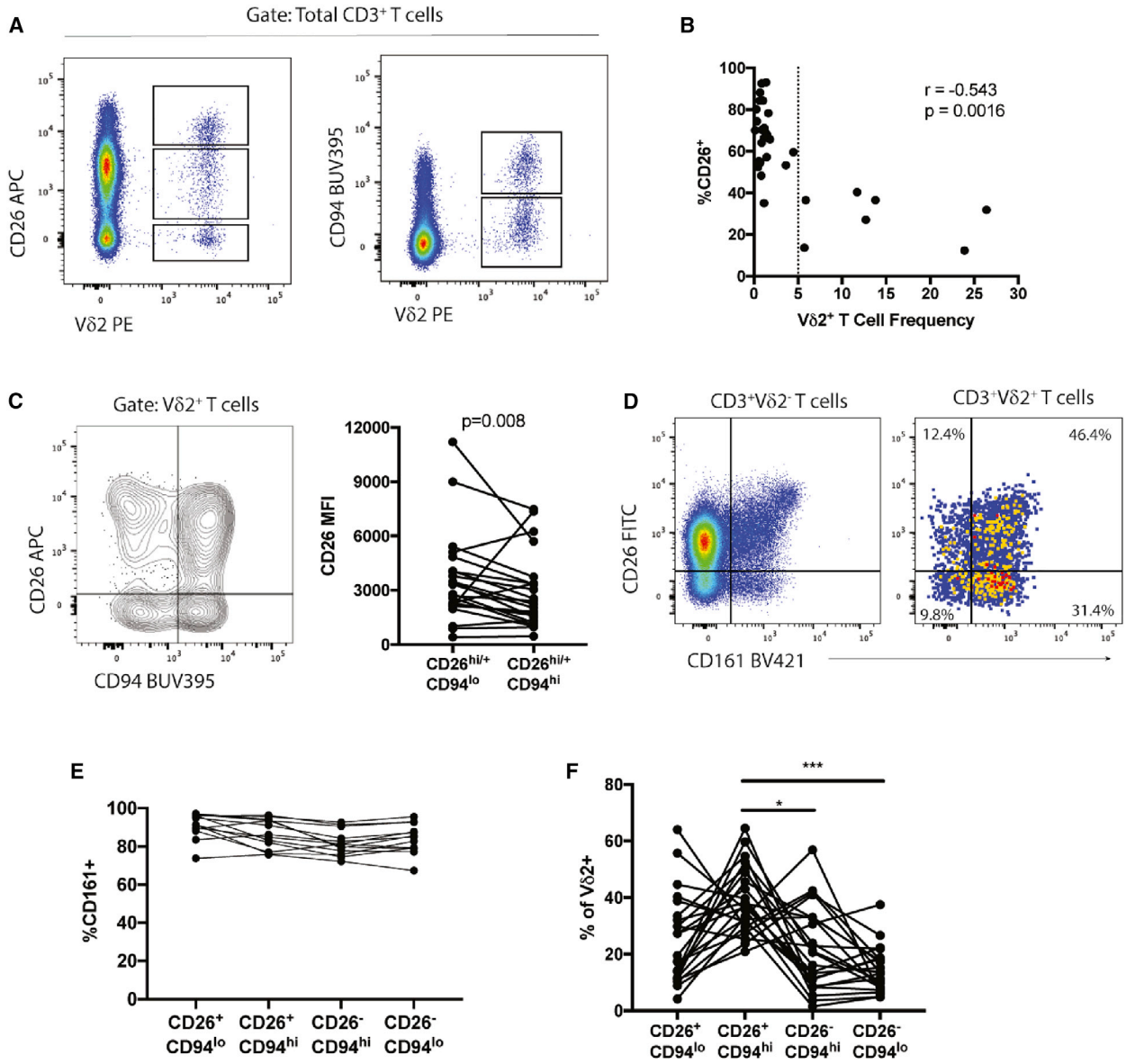

Figure 1. Expression of CD26 and CD94 on Vδ2+ T Cells

(A) Representative staining of CD26 or CD94 expression on Vδ2+ and Vδ2− T cells.

(B) Correlation between *ex vivo* Vδ2+ T cell frequency and the proportion of CD26+ Vδ2+ T cells (n = 32 PBMC donors). Statistics are assessed by Spearman correlation. Dashed line indicates Vδ2+ T cell frequency of 5%.

(C) Representative co-staining of CD26 and CD94 on Vδ2+ T cells. Plot shows quantification of CD26 MFI on CD26-expressing $CD94^{lo}$ and $CD94^{hi}$ subsets. Statistics are assessed by Wilcoxon test.

(D) Representative staining of CD26 and CD161 co-expression among Vδ2+ and Vδ2− T cells.

(E) Quantification of CD161 expression among CD26/CD94 Vδ2+ T cell subsets (n = 13). Statistics are assessed by Friedman test and Dunn's multiple comparisons post-tests.

(F) Comparison of the frequency of CD26/CD94 subsets within the adult Vδ2+ T cell population (n = 23). Statistics are assessed by Friedman test and Dunn's multiple comparisons post-tests. *p < 0.05; ***p < 0.001.

2019) into our analysis of the four CD26/CD94 Vδ2+ T cell populations. Using the list of 298 DRGs identified in Table S1, multidimensionality scaling (MDS) of the 5 cell types suggested that MAIT cells cluster most closely with $CD26^{hi/+}CD94^{lo}$ Vδ2 cells along MDS dimension 1, which defines the majority (>70%) of the dataset variance (Figures S2A and S2B). MAIT cell expression of the Vδ2+ DRGs identified in Figure 2C was highly similar to $CD26^{hi/+}CD94^{lo}$ cells (Figure 2H). To further compare Vδ2+ and MAIT cell transcriptional signatures, we identified the top 20 genes upregulated in MAIT cells compared to CD8+ T cells and again found that $CD26^{hi/+}CD94^{lo}$ cells were transcriptionally similar to MAIT cells (Figure S2C). Using the MAIT/CD8 and

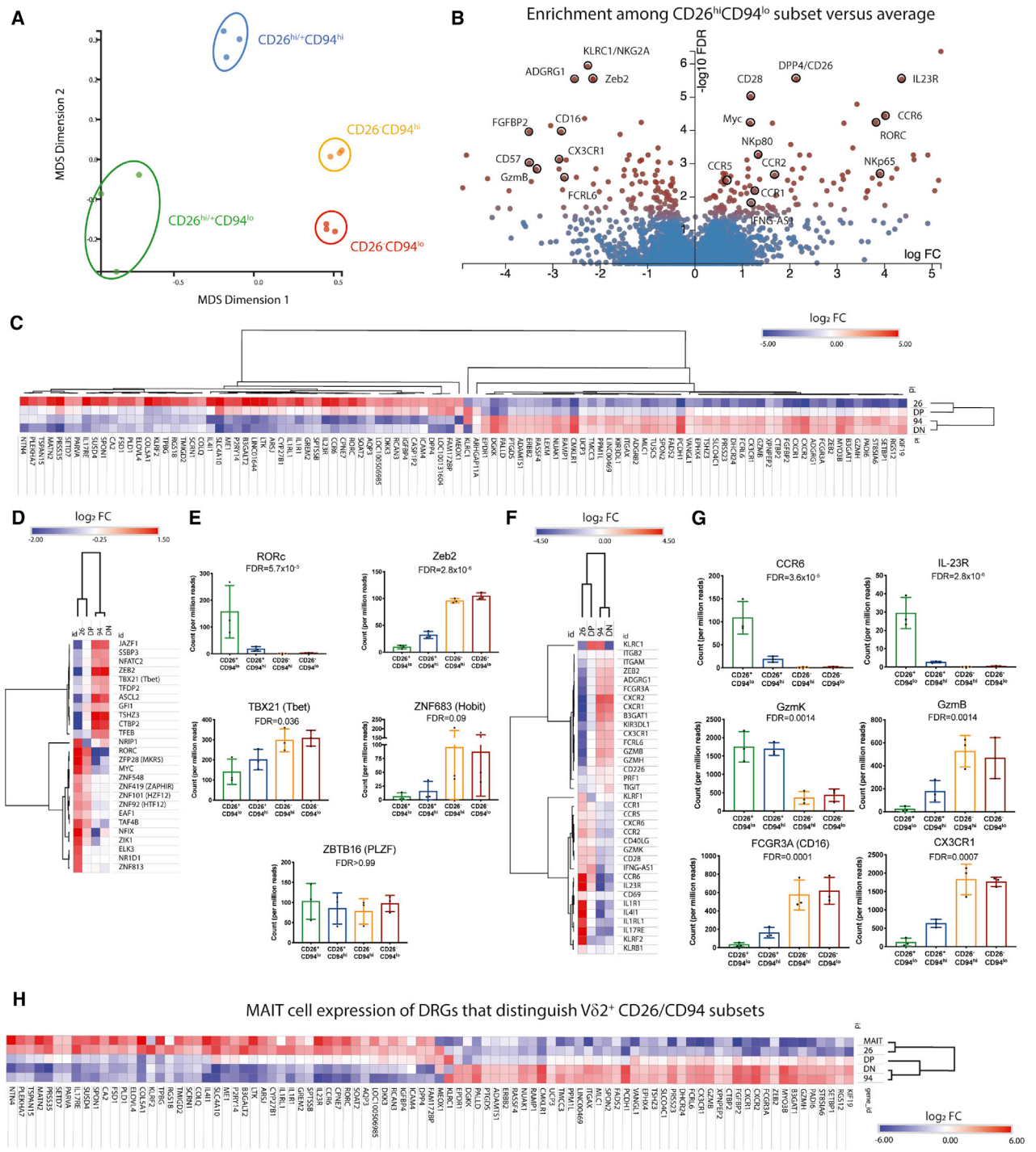

Figure 2. RNA Sequencing of CD26/CD94 Vδ2$^+$ T Cell Subsets

(A) RNA was extracted from sorted CD26/CD94 Vδ2$^+$ T cells derived from three healthy donors. Multidimensionality scaling (MDS) plot indicates clustering of samples based on differentially regulated genes.

(B) Volcano plot displaying the log fold change (logFC) and −log10 FDR of all transcripts identified by RNA sequencing for the CD26$^{hi/+}$CD94^{lo} population relative to the average of all samples. Red indicates FDR < 0.05. Selected immune-related transcripts are annotated.

(C) Heatmap of the top 50 upregulated and top 50 downregulated genes (by FC) in the CD26$^{hi/+}$CD94^{lo} population relative to the average of all four populations. "26," sorted CD26$^{hi/+}$CD94^{lo} population; "DP," CD26$^{hi/+}$CD94^{hi} cells; "94," CD26^{-}CD94^{hi} cells; "DN," CD26^{-}CD94^{lo} cells. Scale indicates log FC compared to the average of all samples. Genes and CD26/CD94 populations were clustered by hierarchical clustering.

(legend continued on next page)

CD26/CD94 datasets, we were able to identify a set of 55 genes that reliably distinguished the MAIT cell and CD26$^{hi/+}$CD94^{lo} Vδ2$^+$ subset from all other Vδ2$^+$ and CD8$^+$ T cells (Figure S2D). Overall, the data suggest that CD26/CD94 Vδ2$^+$ subsets are transcriptionally distinct, and CD26$^{hi/+}$CD94^{lo} cells exhibit similar transcriptional profiles to MAIT cells.

CD26^{hi}CD94^{lo} Vδ2$^+$ Cells Are Not MR1 Restricted

To compare the phenotypic characteristics of Vδ2$^+$ and MAIT cells, we defined four Vδ2$^+$ subsets based on the co-expression of CD26 and CD94: CD26^{hi}CD94^{lo}; CD26$^+$CD94^{hi}; CD26$^-$CD94^{hi}; and CD26$^-$CD94^{lo} (Figures S3A–S3C). Staining of CD26 and CD94 on MR1 5-OP-RU tetramer$^+$ cells (MR1 tet$^+$) confirmed previous reports that the majority of MAIT cells are CD26^{hi} and CD94^{lo} (median 89.2%; Figure S3C). Interestingly, expression of CD94 on MR1 tet$^+$ cells was not associated with CD26 downregulation (Figure S3C). Although the majority of CD26^{hi} MR1 tet$^+$ cells were PLZF$^+$, CD26$^{+/-}$ cells expressed highly variable levels of PLZF, consistent with previous observations of CD26$^-$ "non-MAIT-like" MR1 tet$^+$ cells (Koay et al., 2019). In contrast, all four Vδ2$^+$ CD26/CD94 subsets were predominately PLZF$^+$ (Figures S3D and S3E). Despite their transcriptional similarities, co-staining of peripheral blood mononuclear cells (PBMCs) confirmed that MR1 tet$^+$ and Vδ2$^+$ cells are distinct populations (Figure S3C). Within the CD3$^+$Vδ2$^+$ T cell population, only a median of 0.09% of Vδ2 cells exhibited any binding to the MR1 tetramer (Figure S3F), with no evidence to suggest any bias toward a particular CD26/CD94 phenotype among the small population of co-staining cells (Figure S3F). Thus, we conclude that CD26^{hi}CD94^{lo} Vδ2$^+$ T cells are not MR1 restricted, consistent with the recent report by Le Nours et al. (2019), in which only Vδ1, Vδ3, and Vδ5 TCRs were shown to bind MR1.

CD26/CD94 Expression Discriminates between MAIT-like and Cytotoxic Vδ2$^+$ T Cells

We next compared the phenotype of CD26^{hi}CD94^{lo} Vδ2$^+$ T cells to other Vδ2$^+$ subsets and CD26^{hi} MR1 tet$^+$ subsets, focusing on immune-related proteins identified by RNA-seq or known to be expressed on MAIT and Vδ2$^+$ cells (Figures 3A and S4A). Similar to MAIT cells, CD26^{hi}CD94^{lo} Vδ2$^+$ cells preferentially expressed CCR6 and exhibited the highest expression of IL-18Rα, CCR5, and CD127 among the Vδ2$^+$ T cell population. Despite the near-homogeneous expression of DNAM-1 (CD226) by CD26$^{+/-}$ Vδ2$^+$ cells, both MAIT and CD26^{hi}CD94^{lo} Vδ2$^+$ cells exhibited clear DNAM-1$^-$ and DNAM-1$^+$ subsets. Steady-state expression of GzmB is a distinguishing feature of Vδ2 T cells compared to resting MAIT cells, which express GzmK, but not GzmB (Kurioka et al., 2015). We found that, although both MR1 tet$^+$ and CD26^{hi}CD94^{lo} Vδ2$^+$ cells express high levels of GzmK (Figures 3A and S4A), GzmB expression is largely restricted to Vδ2$^+$ CD26$^+$CD94^{hi} and CD26$^-$ cells (Figures 3A and S4A). Consistent with a lack of steady-state effector profile, both MAIT and CD26^{hi}CD94^{lo} Vδ2$^+$ cells were negative for CD16, CX3CR1, and CD57 expression (Figures 3A and S4A).

Further similarities between MAIT and CD26^{hi} Vδ2$^+$ cells were found in the expression of key transcription factors. CD26^{hi}CD94^{lo} cells heterogeneously expressed Helios and were Tbet^{dim}Eomes^{hi}, similar to our and others' analysis of MR1 tet$^+$ cells (Leeansyah et al., 2015; Figures 3A and S4B). We confirmed the preferential expression of Hobit and Zeb2 among CD26$^-$ Vδ2$^+$ cells at the protein or mRNA (for Zeb2) level (Figures 3A, S4B, and S4C). Expression of these transcription factors was similarly low in MR1 tet$^+$ cells (or CD8$^+$CD26^{hi} cells in the Zeb2 PrimeFlow assay). Despite detection of RORc RNA expression in the RNA-seq dataset, we were unable to find any evidence for protein expression of RORγt in CD26^{hi}CD94^{lo} Vδ2$^+$ T cells (Figure 3A), consistent with previous studies (Provine et al., 2018) and likely explaining the poor IL-17 production by adult Vδ2$^+$ T cells *ex vivo*.

The expression patterns of several transcription factors and GzmB were suggestive of a continuum of differentiation from a MAIT-like phenotype among CD26^{hi}CD94^{lo} cells to an effector-like phenotype among CD26$^-$ cells. Compared to the CD26^{hi}CD94^{lo} population, CD26$^+$CD94^{hi} cells exhibit intermediate Tbet and Eomes expression, although CD26$^-$CD94^{hi} and CD26$^-$CD94^{lo} cells are predominately Tbet^{hi}Eomes^{low} (Figures 3B and S4D). Similarly, GzmB, Hobit, and Zeb2 expression are progressively upregulated as CD26 expression declines (Figure 3C), suggesting a link between CD26 downregulation and differentiation toward cytotoxic Vδ2$^+$ effector cells.

CD26/CD94 Expression Does Not Recapitulate Conventional T Cell Memory Subsets

Angelini et al. (2004) and Ryan et al. (2016) have previously shown that CD16 expression and cytotoxic function of Vδ2$^+$ T cells are associated with a CD27$^-$CD45RA$^+$ effector memory (T_{EMRA}) phenotype. This led us to assess whether CD26$^+$ and CD26$^-$ Vδ2$^+$ T cell subsets were simply identifying central (T_{CM} or CD27$^+$) versus effector memory (T_{EM} or CD27$^-$) phenotypes. Consistent with other studies (Davey et al., 2018), the majority of both Vδ2$^+$ and MR1 tet$^+$ T cells in our cohort exhibited a CD27$^+$CD45RA$^-$ phenotype (Figure 4A). Segregation of Vδ2$^+$ T cells based on CD27 expression demonstrated that all four CD26/CD94 subsets exist within the CD27$^+$ subpopulation but that CD27$^-$ cells were enriched for CD26$^-$CD94$^+$ cells (Figure 4B). These data are consistent with previous observations of high GzmB and CD16 expression within CD27$^-$ Vδ2 cells

(D) Heatmap of all transcription factors identified in the 298 differentially expressed transcripts. Scale indicates log fold change compared to the average of all samples.
(E) Comparison of transcript reads for selected transcription factor genes between CD26/CD94 subsets.
(F) Heatmap of immune-related genes in the 298 differentially expressed transcripts. Scale indicates log FC compared to the average of all samples.
(G) Comparison of transcript reads between CD26/94 subsets for selected genes from (F).
(H) Heatmap of the 100 DEGs from (C), using a combined dataset that includes the CD26/CD94 Vδ2$^+$ subsets and published RNA transcriptome data from sorted human MAIT cells (n = 3 donors; Hinks et al., 2019). Heatmap shows log FC relative to the average of all samples. Cell populations were clustered by hierarchical clustering.

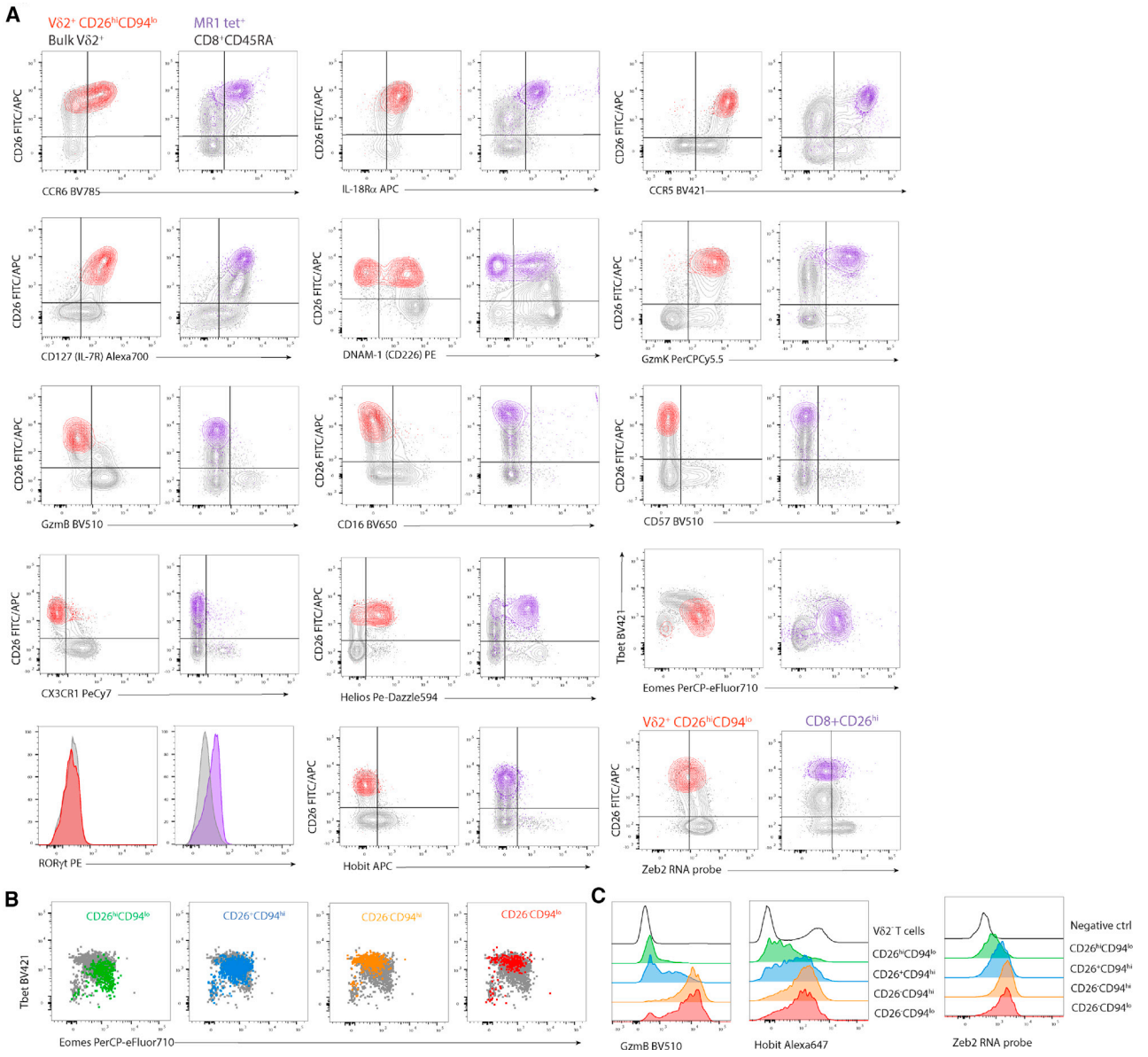

Figure 3. Phenotypic Profile of CD26^{hi}CD94^{lo} Vδ2^{+} T Cells

(A) Comparison of surface or intracellular protein expression among CD26^{hi}CD94^{lo} (red) and bulk Vδ2^{+} T cells (gray) or MR1 tet^{+} cells (purple) and CD8^{+}CD45RA^{-} cells (gray). Plots are representative of 12–17 PBMC donors for each marker or 6 donors for Zeb2.

(B) Representative co-expression of Tbet and Eomes among Vδ2^{+} T cell CD26/CD94 subsets (color) compared to bulk Vδ2^{+} T cells (gray; representative of 15 donors).

(C) Representative expression of GzmB, Hobit, and Zeb2 among Vδ2^{+} T cell CD26/CD94 subsets.

but suggest that a spectrum of Vδ2^{+} T cell phenotypes defined by CD26/CD94 expression exists within the CD27^{+} compartment and that acquisition of a cytotoxic phenotype may be uncoupled from terminal differentiation.

Ryan et al. (2016) also demonstrated an enrichment of CCR6 and IL-18Rα expression among CD28^{+}CD27^{+}CD45RA^{-} Vδ2^{+} T cells, as well as distinct expression patterns of CCR6 and CX3CR1. In our cohort, CD28 was highly expressed by both the CD26^{hi}CD94^{lo} and CD26^{+}CD94^{hi} populations, as well as MR1 tetramer^{+} cells (Figure 4C). Critically, however, CD26^{hi}CD94^{lo} cells accounted for only a median of 16.7% of the CD27^{+}CD28^{+} Vδ2 population (Figure 4D), demonstrating that CD28 is not a sufficient proxy to identify the MAIT-like CD26^{hi}CD94^{lo} Vδ2^{+} T cell subset. We further confirmed that CD26^{hi}CD94^{lo} Vδ2 T cells are significantly enriched for CCR6 and IL-18Rα expression but exclude CX3CR1^{+} cells compared to CD27^{+}CD28^{+} cells in a direct comparison of the two Vδ2 populations (Figure 4E).

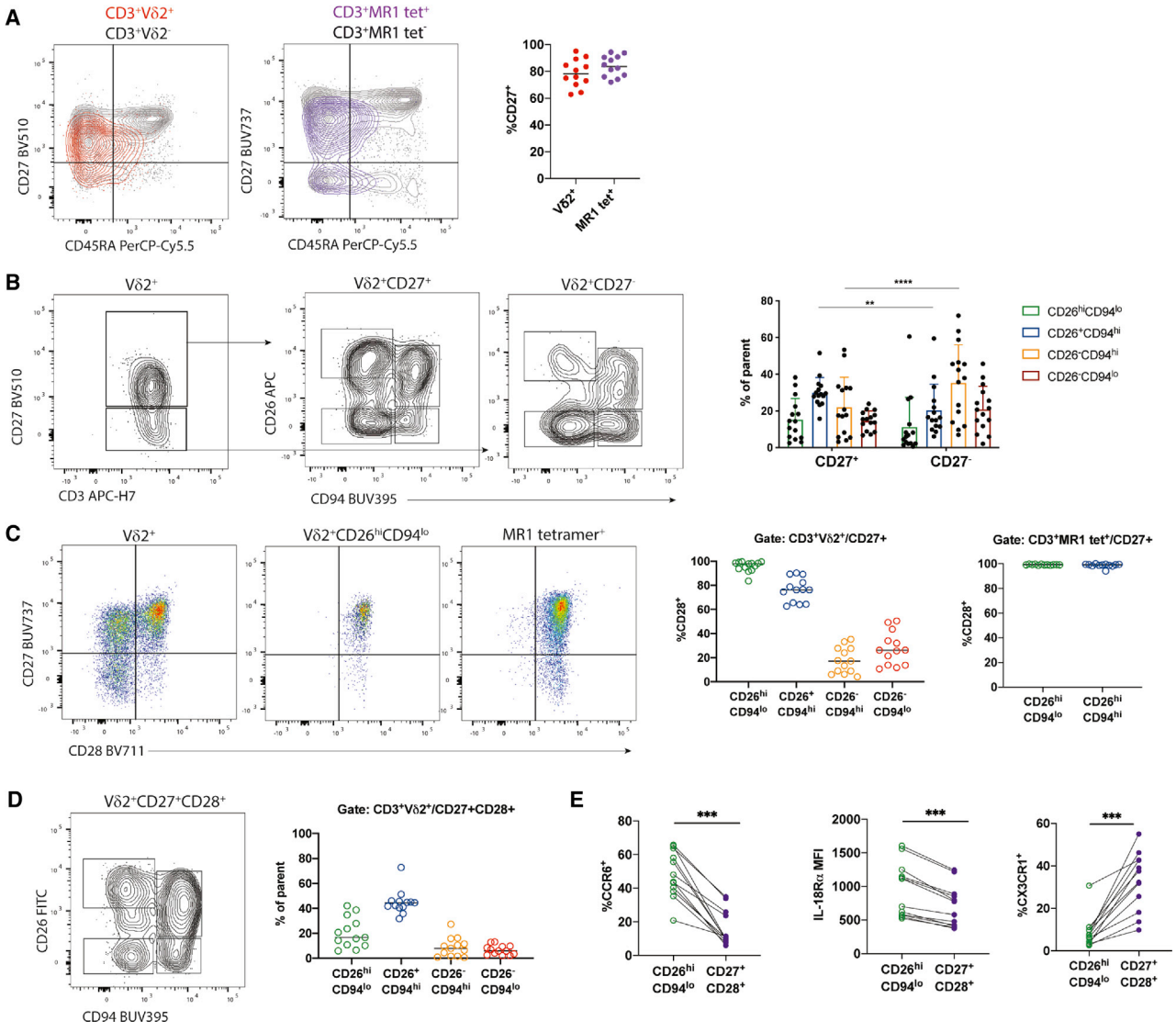

Figure 4. Comparison of CD26/CD94 Phenotype and Memory Status

(A) Representative staining of CD27 and CD45RA expression on Vδ2$^+$ T cells (red) compared to Vδ2$^-$ T cells (gray) or MR1 tet$^+$ cells (purple) compared to MR1 tet$^-$ T cells (gray). Plot indicates frequency of CD27$^+$ Vδ2$^+$ T cells or MR1 tet$^+$ T cells among n = 12 PBMC donors.

(B) Representative staining and quantification (n = 15) of CD26/CD94 subset frequency among CD27$^+$ and CD27$^-$ Vδ2$^+$ T cells. Statistics are assessed by two-way ANOVA with Sidak's multiple comparisons post-test.

(C) Representative staining of CD27 and CD28 co-expression among bulk Vδ2$^+$ T cells, CD26^{hi}CD94^{lo} Vδ2 T cells, and MR1 tet$^+$ T cells. Plots indicate the frequency of CD28$^+$ cells among each Vδ2$^+$CD27$^+$ (n = 13) or MR1 tet$^+$CD27$^+$ T cell subset (n = 12).

(D) Representative staining of CD26 and CD94 subsets within the Vδ2$^+$CD27$^+$CD28$^+$ population. Plot shows the frequency of each CD26/CD94 subset within the Vδ2$^+$CD27$^+$CD28$^+$ gate (n = 13).

(E) Comparison of CCR6, IL-18Rα, and CX3CR1 expression on CD26^{hi}CD94^{lo} or CD27$^+$CD28$^+$ Vδ2$^+$ subsets (n = 12). Statistics are assessed by Wilcoxon test. **p < 0.01; ***p < 0.001; ****p < 0.0001. Lines indicate medians.

CD26$^+$CD94^{hi} Vδ2$^+$ T Cells Are Enriched for IL-12/IL-18 Responsiveness

Because IL-18Rα MFI was highest among CD26^{hi}CD94^{lo} cells (Figure 3A), we anticipated that these cells would represent the major cytokine-responsive Vδ2$^+$ T cell subset. Unexpectedly, however, CD26$^+$CD94^{hi} cells were significantly more likely to produce IFNγ in response to IL-12/IL-18 stimulation compared to other Vδ2$^+$ T cell subsets (Figure 5A). We confirmed in matched data from 7 donors that, despite significantly higher IL-18Rα expression on CD26^{hi}CD94^{lo} cells *ex vivo*, the CD26$^+$CD94^{hi} subset was significantly more likely to produce IFNγ in response to IL-12+IL-18 stimulation (Figure 5B; p = 0.0156 and 0.0312, respectively). This mirrors observations that CD94 expression is associated with cytokine responsiveness on NK cells (Yu et al., 2010) and MAIT cells (Dias et al., 2017), and the transcriptional data provide two potential

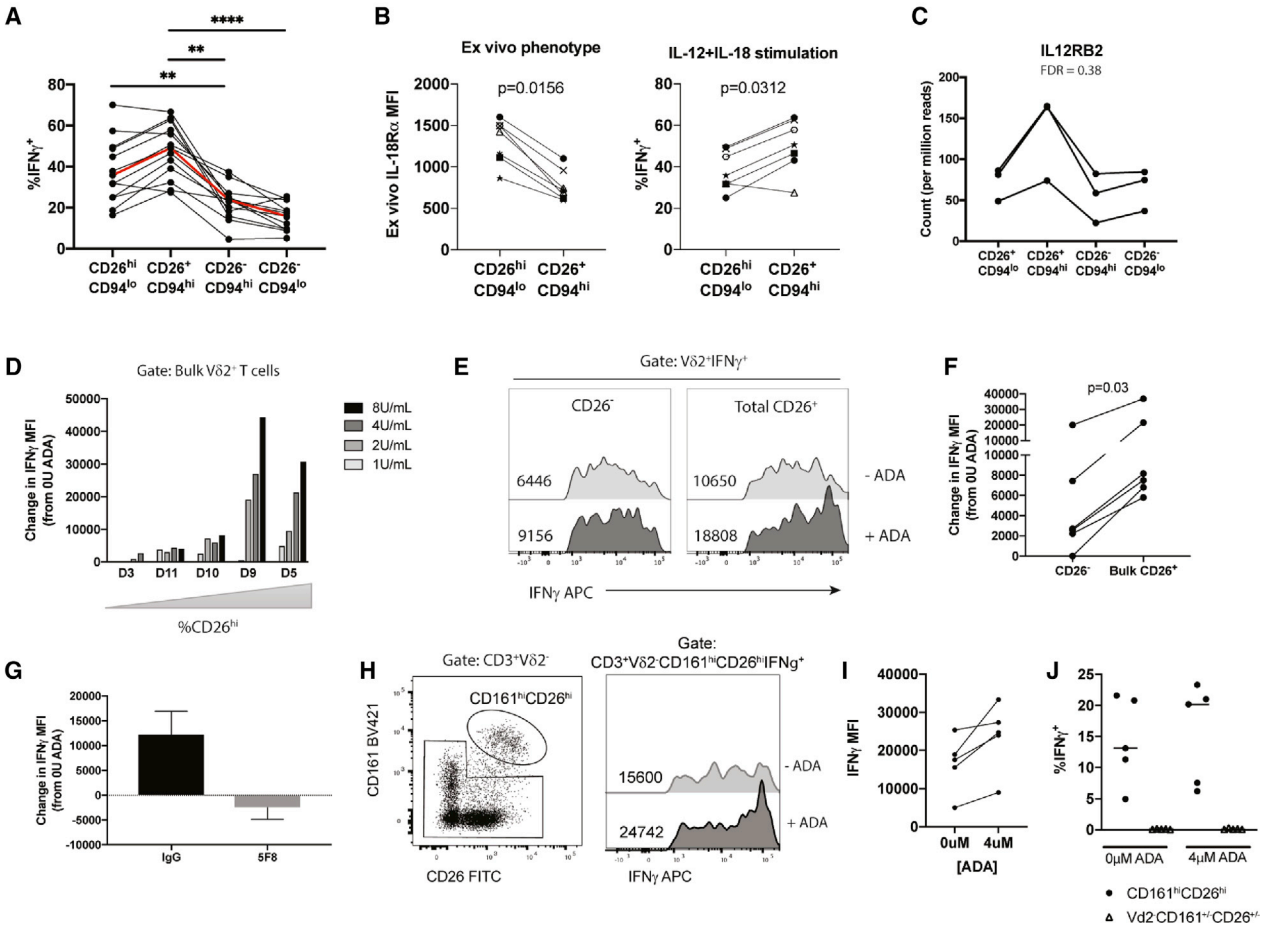

Figure 5. CD26^{+}CD94^{hi} Cells Are Highly Responsive to IL-12 and IL-18 Stimulation

(A) Cytokine-induced IFNγ expression was quantified among CD26/CD94 Vδ2^{+} T cells (n = 13). Statistics are assessed by Friedman test and Dunn's post-test.

(B) Comparison of *ex vivo* IL-18Rα MFI and IL-12/IL-18-induced IFNγ expression between CD26^{hi}CD94^{lo} and CD26^{+}CD94^{hi} subsets in 7 paired samples (symbols indicate individual donors). Statistics are assessed by Wilcoxon test.

(C) IL-12RB2 mRNA expression across CD26/CD94 subsets from the RNA-seq dataset described in Figure 2.

(D) MFI of IFNγ staining among IFNγ^{+}Vδ2^{+} T cells among stimulation cultures with or without ADA for five PBMC donors.

(E) Histograms depicting IL-12+IL-18-induced IFNγ expression within CD26^{-} or CD26^{+} Vδ2^{+} T cell subsets in the presence or absence of 4 U/mL ADA. The MFI of IFNγ staining is indicated on the left of each histogram.

(F) Quantification of the ADA-induced increase in IFNγ MFI among CD26^{-} and CD26^{+} Vδ2^{+} T cell subsets in six PBMC donors. Statistics are assessed by Wilcoxon test.

(G) PBMCs were pre-incubated with irrelevant immunoglobulin G (IgG) or anti-CD26 clone 5F8 for 1 h prior to stimulation. The ADA-induced change in IFNγ MFI was calculated for each condition (n = 2 PBMC donors).

(H) Gating of CD161^{2+}CD26^{2+} T cells within the CD3^{+}Vδ2^{-} population. Histograms show IFNγ expression following IL-12/IL-18 stimulation in the presence or absence of ADA for CD3^{+}Vδ2^{-}CD161^{2+}CD26^{2+} T cells (IFNγ MFI is indicated on each histogram).

(I) Quantification of the ADA-induced increase in IFNγ MFI among CD161^{2+}CD26^{2+} T cells in five PBMC donors.

(J) IFNγ responses to IL-12/IL-18 stimulation in the presence or absence of ADA for CD161^{2+}CD26^{2+} T cells or CD3^{+}Vδ2^{-}CD161$^{+/-}$CD26$^{+/-}$ cells. Lines indicate medians.

mechanisms for this observation. First, the RNA-seq data indicated a possible enrichment of IL-12RB2 mRNA within the CD26^{+}CD94^{hi} subset compared to other Vδ2^{+} T cells (Figure 5C), although this observation requires confirmation in a larger number of donors at the protein level. Second, as noted above, Tbet expression was consistently higher among CD26^{+}CD94^{hi} cells compared to CD26^{+}CD94^{lo} cells (as shown in Figures 3B and S4B). Interestingly, there was no enhancement of IFNγ, tumor necrosis factor (TNF), or GM-colony stimulating factor (CSF) production by the CD26^{+}CD94^{hi} subset in response to HMB-PP stimulation compared to other Vδ2 cells (not shown).

CD26 Enhances Vδ2^{+} T Cell Cytokine Responsiveness via Adenosine Deaminase Binding

Given the multifunctional nature of CD26, we assessed whether the adenosine deaminase (ADA) binding capacity of the CD26 protein could promote TCR-independent responsiveness. Incubation of PBMCs with recombinant ADA during IL-12+IL-18

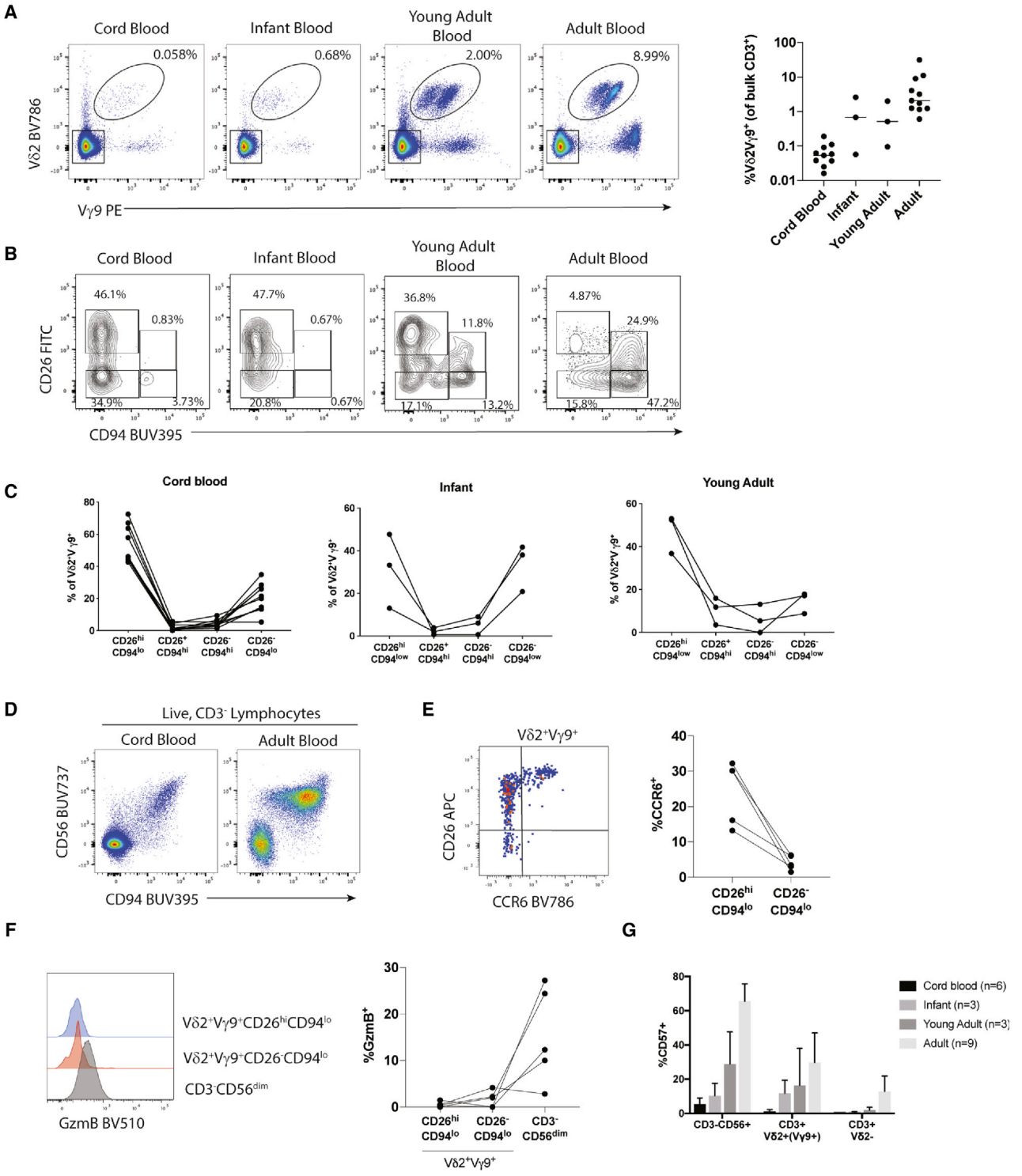

Figure 6. Vδ2$^+$Vγ9$^+$ Cell CD26/CD94 Co-expression on Cord Blood and Infant/Young Adult PBMC Samples

Infant samples were defined as age <1 year, young adult as age between 1 and 14 years, and adult samples age >20 years.

(A) Representative staining of Vδ2 and Vγ9 TCR expression on CD3$^+$ lymphocytes from CBMC, infant PBMC, young adult PBMC, and contemporaneously stained adult PBMC samples. Circular gate indicates Vδ2$^+$Vγ9$^+$ population. Graph indicates frequency of Vδ2$^+$Vγ9$^+$ T cells among cord blood (n = 10), infant (n = 3), young adult (n = 3), and adult (n = 11) blood samples. One cord blood sample with a Vδ2$^+$Vγ9$^+$ frequency of 0% is not shown.

(legend continued on next page)

stimulation resulted in a dose- and donor-dependent increase in Vδ2$^+$ T cell IFNγ MFI (Figure 5D). Donors with greater proportions of CD26^{2+} Vδ2$^+$ T cells were generally more responsive to ADA than those with fewer CD26^{2+} cells. The ADA-induced increase in IFNγ production was significantly greater among bulk CD26$^+$ Vδ2$^+$ T cells compared to CD26$^-$ cells ($p = 0.03$; Figures 5E and 5F), suggesting that CD26/ADA binding facilitated the increased cytokine production. This was confirmed by pre-incubating PBMCs with 5F8, an antibody that blocks the ADA binding site on CD26 (Abbott et al., 1999), which abrogated the ADA-induced IFNγ increase during cytokine stimulation (Figure 5G). To determine whether CD26/ADA interactions could similarly promote IFNγ expression by other cytokine-responsive CD26^{hi} cells (Ussher et al., 2014), we analyzed IL-12/IL-18 responses by CD3$^+$Vδ2$^-$CD161^{hi}CD26^{hi} cells (Figure 5H). Similar to CD26^{hi} Vδ2$^+$ cells, ADA promoted IFNγ expression in the CD161^{hi}CD26^{hi} T cell population (Figures 5H and 5I). No other T cell subsets were observed to respond to IL-12/IL-18+ADA stimulation (Figure 5J).

CD94 Is Co-expressed with Either NKG2A or NKG2C on Vδ2$^+$ T Cells

CD94 could further modify Vδ2$^+$ T cell function through dimerization with either the inhibitory receptor NKG2A or the activating receptor NKG2C, which is upregulated during chronic HCMV and HCMV/HIV co-infection (Gumá et al., 2004, 2006; Mela et al., 2005). All HIV-negative donors exhibited NKG2A expression on CD94^{hi} Vδ2$^+$ T cells (Figure S5A). Even among HCMV-seropositive donors with distinct NKG2C$^+$ NK and T cell populations, we were unable to detect a convincing CD94$^+$NKG2C$^+$ Vδ2$^+$ T cell subset (Figure S5A). The relationship between high-density CD94 and NKG2A expression in HCMV-seropositive donors was also confirmed in the RNA-seq data (Figure S5B). Cross-linking of NKG2A during a CD3-induced redirected lysis assay confirmed that NKG2A negatively regulates Vδ2$^+$ T cell function immediately *ex vivo*, without the need for any priming or cytokine exposure (Figures S5C–S5E). In contrast, NKG2A cross-linking had no inhibitory impact on HMB-PP-induced cytokine production (Figure S5F).

Given the expansion of NKG2C$^+$ NK cells in HIV-infected cohorts compared to HIV-negative HCMV$^+$ donors (Mela and Goodier, 2007), we examined CD26/CD94 expression among a cohort of HIV-infected participants (Immunovirology Research Network [IVRN] cohort) initiating antiretroviral therapy (ART) (demographics shown in Table S2). A substantial proportion of HIV-infected ART-naive individuals exhibited low levels of Vδ2$^+$ CD26 expression (<50%) compared to healthy individuals with similar Vδ2$^+$ T cell frequencies, which was only partially restored by suppressive ART (Figure S5G). Despite the changes in Vδ2$^+$ T cell phenotype and the expansion of NKG2C$^+$ NK cells in this cohort (Figure S5H), only one of 24 participants exhibited a convincing NKG2C$^+$ Vδ2$^+$ T cell population (Figure S5I). To extend this result, we screened a second cohort of ART-treated participants and identified an additional 3 donors (out of 27 participants) with distinct CD94$^+$NKG2C$^+$ subsets (Figure S5I). Three out of the four donors exhibited sufficient Vδ2$^+$NKG2C$^+$ events for further phenotyping, which revealed that the NKG2C$^+$ Vδ2$^+$ T cells were CD26$^-$CD94^{lo} and expressed high levels of CD57 and CD16 (Figures S5J and S5K). Thus, although rare, it is possible for CD26$^-$ Vδ2$^+$ T cells to acquire a NKG2C$^+$CD57$^+$CD16$^+$ phenotype during HIV infection.

Cord Blood Vδ2$^+$Vγ9$^+$ Cells Are Predominately CD26$^+$CD94^{lo}

The presence of CD57 (and rarely NKG2C) on CD26$^-$ Vδ2$^+$ T cells suggests that CD26$^+$ Vδ2$^+$ T cells may represent an immature or undifferentiated cell subset. To test this hypothesis, we assessed the phenotype of Vδ2$^+$Vγ9$^+$ cells in cord blood mononuclear cells (CBMCs) and PBMCs from infants (<1 year old) and young adults (1–14 years old). As expected (Cairo et al., 2008; Berglund et al., 2018), Vδ2$^+$Vγ9$^+$ cells were present at low or undetectable frequencies in cord blood samples but became increasingly prevalent with age (Figure 6A). CD26/CD94 expression patterns in cord blood and infant PBMC samples were strikingly different from those observed in adult PBMC donors; neonates and infants expressed no CD94 on the Vδ2$^+$Vγ9$^+$ population, and the majority of cells were CD26^{hi} or CD26$^+$ (Figures 6B and 6C versus Figure 1F). Overall, the CD26^{hi}CD94^{lo} population accounted for a median of 46.05% of cord blood Vδ2$^+$Vγ9$^+$ cells (Figures 6B and 6C) compared with a median of 19.5% in adults. This pattern persisted in infants, as only young adult PBMC samples began to exhibit CD94^{hi} Vδ2$^+$ T cells (Figures 6B and 6C). The absence of CD94^{hi} Vδ2$^+$Vγ9$^+$ T cells in neonates and infants was not due to a generalized lack of CD94 expression, as CD3$^-$CD56$^+$ NK cells expressed levels of CD94 comparable to adult NK cells (Figure 6D). Similar to adult CD26^{hi}CD94^{lo} Vδ2$^+$ cells, CCR6 expression among cord blood Vδ2$^+$Vγ9$^+$ cells was restricted to the CD26^{hi} subset (Figure 6E). Notably, however, CD26$^-$CD94^{lo} cord blood cells were not GzmB$^+$ (in contrast to cord blood NK cells; Figure 6F). Consistent with previous observations, we found that NK and conventional T cell expression of CD57 was negligible in neonates and increased with age; a similar pattern was observed

(B) Representative staining of CD26 and CD94 expression patterns among cord blood, infant, young adult, and adult CBMC/PBMC samples. CD94^{hi} gate was set based on contemporaneously stained adult PBMC samples.
(C) Quantification of CD26/CD94 subset distribution among Vδ2$^+$Vγ9$^+$ cells from cord blood (n = 10 samples with detectible Vδ2$^+$Vγ9$^+$ population), infant (n = 3), and young blood (n = 3).
(D) Representative staining of CD94 expression on CD3$^-$CD56$^+$ lymphocytes in one cord blood and one adult blood sample (data are representative of n = 10 CBMC and n = 3 adult samples).
(E) Representative staining and quantification of CCR6 expression on cord blood Vδ2$^+$Vγ9$^+$ T cells (n = 5).
(F) Representative staining and quantification GzmB expression among cord blood CD26^{hi}CD94^{lo} and CD26$^-$CD94^{lo} Vδ2$^+$Vγ9$^+$ T cells or CD3$^-$CD56^{dim} NK cells (n = 5).
(G) Quantification of CD57 expression on CD3$^-$CD56$^+$ NK cells, CD3$^+$Vδ2$^+$Vγ9$^+$ cells, and CD3$^+$Vδ2$^-$ cells. n = 6 for cord blood samples except for CD3$^+$Vδ2$^+$Vγ9$^+$ cells, where n = 5.

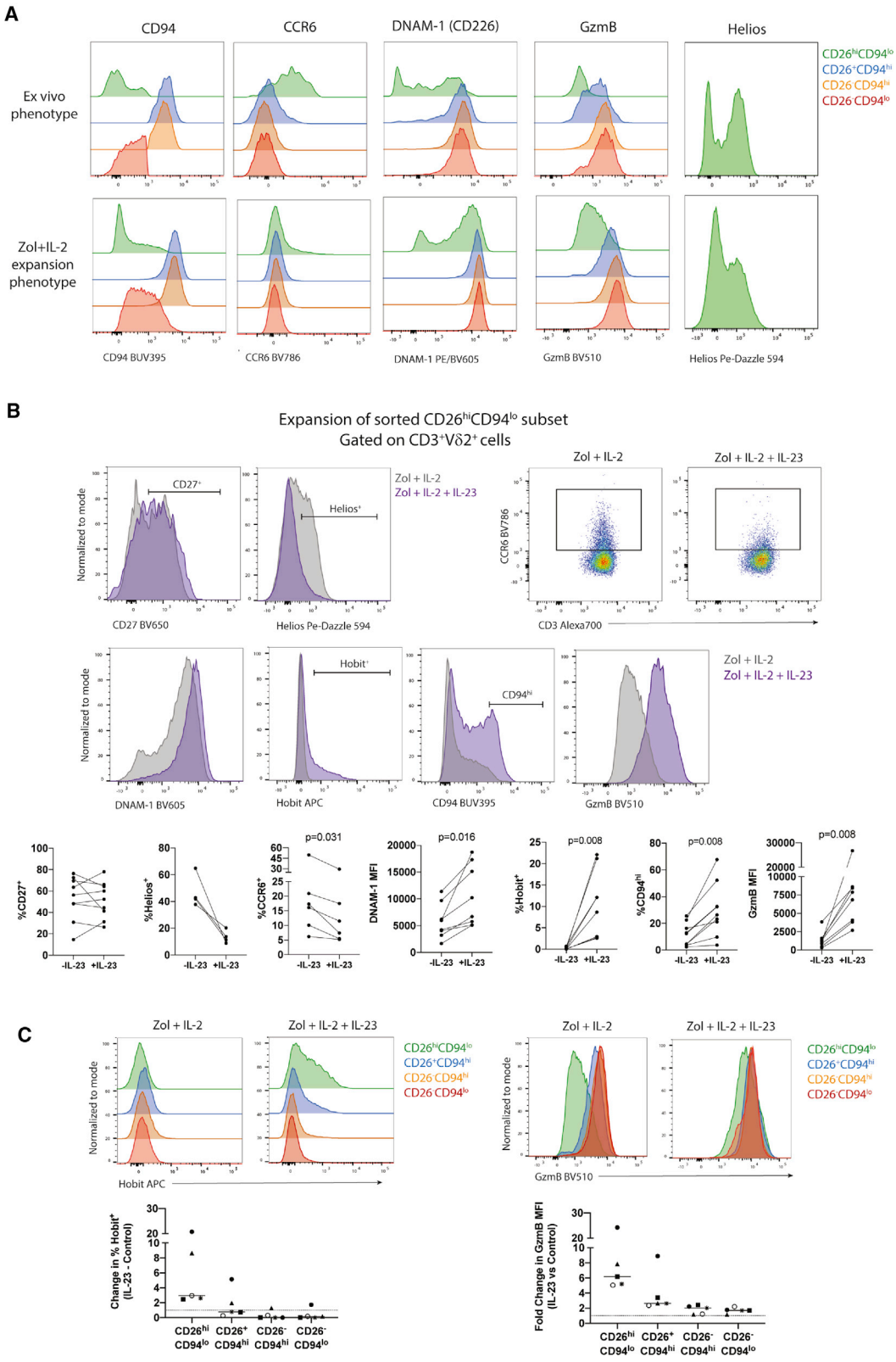

(legend on next page)

for Vδ2$^+$Vγ9$^+$ cells, suggesting that CD57 does indeed represent a marker of differentiation on these cells (Figure 6G).

Exposure to Antigen and IL-23 Drives CD26^{hi}CD94^{lo} Vδ2$^+$ Cells toward a Cytotoxic Effector Phenotype

Given the distinct CD26/CD94 profiles of Vδ2$^+$ T cells between cord and adult blood samples, we aimed to determine whether the CD26^{hi}CD94^{lo} population could act as a progenitor of any of the other subsets. First, we extracted TCR CDR3 sequences from the *ex vivo* RNA-seq data to investigate the clonotypic relationship of the CD26/CD94 subsets. Shared CDR3 clonotypes between Vδ2$^+$ subsets were observed in all three donors (Figure S6A), with up to 20 clonotypes being present in all four subsets (Figure S6B). These data suggest that, in adults, Vδ2$^+$ clonal expansion is associated with *in vivo* transitions in CD26/CD94 phenotype.

To specifically investigate the impact of antigen stimulation and proliferation on each CD26/CD94 subset, we sorted CD26^{hi}CD94^{lo}, CD26$^+$CD94^{hi}, CD26$^-$CD94^{hi}, and CD26$^-$CD94^{lo} Vδ2$^+$ T cell subsets and cultured them in the presence of autologous γδ-depleted PBMCs, zoledronate (zol), and IL-2 (Figures S7A and S7B). Following *in vitro* expansion, CD26^{hi}CD94^{lo} cells retained a number of their unique characteristics, including CCR6 and Helios expression, as well as lower CD94, DNAM-1, and GzmB MFI compared to the other three subsets (Figure 7A and as previously shown in Figure S4). Thus, 14-day expansion of CD26^{hi}CD94^{lo} cells in the presence of antigen and IL-2 upregulated GzmB but did not induce many of the characteristics of CD26$^{+/-}$ Vδ2$^+$ T cells.

IL-23/IL-23R signaling has recently been shown to promote the proliferation and activation of MAIT cells (Wang et al., 2019). Given that CD26^{hi}CD94^{lo} Vδ2$^+$ T cells similarly express IL-23R, we assessed the impact of IL-23 exposure on zol/IL-2-mediated Vδ2$^+$ T cell expansion. Strikingly, CD26^{hi}CD94^{lo} cells expanded in the presence of IL-23 markedly differed in phenotype from those expanded under typical conditions; although CD27 expression was maintained, Helios and CCR6 expression declined, and DNAM-1, Hobit, CD94, and GzmB were upregulated (Figure 7B). Importantly, the impact of IL-23 was largely restricted to the CD26^{hi}CD94^{lo} subset; it had a minor effect to upregulate Hobit and GzmB on CD26$^+$CD94^{hi} cells and minimal impact on either CD26$^-$ subset (Figure 7C).

To more comprehensively characterize the impact of IL-23 exposure on CD26/CD94 subsets, we performed a transcriptomic analysis of each subset, expanded with either zol and IL-2 or zol, IL-2, and IL-23, from two independent experiments (MDS shown in Figure S7C). The transcriptome analysis confirmed our previous observation that many defining characteristics of each Vδ2$^+$ subset are maintained following expansion, as the expression of DRGs from our *ex vivo* RNA-seq experiment (Figure 1C) retained similar expression patterns among the four populations after expansion with zol/IL-2 (Figure S7D; Table S3). More importantly, the RNA-seq data clearly demonstrated the differential impact of IL-23 exposure among the CD26/CD94 subsets. 1,503 genes were differentially regulated by IL-23 among the CD26^{hi}CD94^{lo} cells, compared to 428 genes in the CD26$^+$CD94^{hi} subset and only 5 genes in the CD26$^-$ subsets (Figure S7E). The IL-23-related DRGs included a number of genes previously identified as being associated with the MAIT-like transcriptional signature or as differentiating the CD26/CD94 subsets *ex vivo* (Figure S7E). Critically, these genes were regulated by IL-23 in a manner that shifted the CD26^{hi}CD94^{lo} transcriptional profile toward that of CD26$^-$ Vδ2$^+$ cells (Figure S7F), consistent with our flow cytometry analysis.

Although many of the characteristics of CD26$^-$ Vδ2$^+$ T cells could be induced in CD26^{hi} cells following IL-23 treatment, neither cytokines or antigen exposure resulted in the loss of CD26 surface expression (Figure S7G). Early studies of CD26 regulation, however, suggested that brief ligation of CD26 induced long-term CD26 downregulation on T cells (Dang et al., 1990). We found that 1 h of exposure to the activating anti-CD26 antibody, 1F7, induced substantial CD26 downregulation on Vδ2$^+$ T cells that was maintained for at least 3 days in cell culture (Figure S7H). In contrast, the non-activating antibody 5F8 had a minimal impact on CD26 surface expression (Figure S7H). Even in the context of strong antigen/IL-2 stimulation during 14-day *in vitro* bulk Vδ2$^+$ T cell expansions, addition of 1F7 to the culture on days 6–9 had a lasting impact on CD26 surface density measured at day 14 of culture (Figure S7I). This 1F7-mediated CD26 downregulation was substantially enhanced when CD26^{hi}CD94^{lo} sort-purified cells were expanded in the presence of IL-23 (Figure S7J). Compared to expansion with zol and IL-2 alone, the expansion of CD26^{hi}CD94^{lo} cells with zol, IL-2, IL-23, and 1F7 resulted in the generation of CD26$^-$CD94$^{hi/lo}$ cells that were homogenously DNAM-1$^+$, Helios$^-$, and GzmB$^+$ and expressed Hobit (Figure S7J). Thus, the combination of IL-23 exposure and CD26 engagement causes CD26^{hi}CD94^{lo} Vδ2$^+$ T cells to phenocopy many of the characteristics and transcriptional features of the CD26$^-$ Vδ2$^+$ T cell subset observed *ex vivo*.

DISCUSSION

Despite completely distinct TCR specificities, CD26^{hi}CD94^{lo} Vδ2$^+$ T cells and CD26^{hi} MAIT cells share a transcriptional profile characterized by high cytokine responsiveness, CCR6 expression, and low steady-state expression of GzmB and other effector molecules. The CD26^{hi}CD94^{lo} phenotype dominates

Figure 7. *In Vitro* Expansion and Differentiation of CD26/CD94 Vδ2$^+$ T Cell Subsets

(A) Histograms show expression of CD94, CCR6, DNAM-1, GzmB, and Helios on CD26^{hi}CD94^{lo} (green), CD26$^+$CD94^{hi} (blue), CD26$^-$CD94^{hi} (orange), or CD26$^-$CD94^{lo} (red) cells immediately *ex vivo* or following expansion. Results are representative of 4–8 donors for each marker.

(B) Plots show expression of CD27, Helios, CCR6, DNAM-1, Hobit, CD94, and GzmB among expanded CD3$^+$Vδ2$^+$ cells in the IL-2 (gray) or IL-2 and IL-23 (purple) condition. Plots show the quantification of the proportion of positive cells or MFI for each marker (n = 4–9 PBMC donors). Statistics are assessed by Wilcoxon test.

(C) Comparison of Hobit and GzmB expression among all four CD26/CD94 subsets expanded in the presence or absence of IL-23. Plots indicate the change in frequency of Hobit$^+$ cells or fold change in GzmB MFI between IL-23/IL-2 expansion and IL-2 expansion conditions in 5 PBMC donors. Symbols represent matched donors.

the cord blood Vδ2Vγ9 population, although $CD26^{+}CD94^{hi}$, $CD26^{-}CD94^{hi}$, and cytotoxic $CD26^{-}CD94^{lo}$ cells increase in frequency between infancy and adulthood. These data provide additional context to scRNA-seq studies, which have shown that $V\delta2^{+}$ T cells cluster both with MAIT cells and with cytotoxic $CD8^{+}$ T cells (Gutierrez-Arcelus et al., 2019). Interestingly, $CD26^{hi}CD94^{lo}$ $V\delta2^{+}$ T cells can be induced to express many markers and transcription factors characteristic of the *ex vivo* $CD26^{-}$ $V\delta2^{+}$ population. Both our results and those of Ryan et al. (2016) suggest that phosphoantigen exposure alone is insufficient to drive peripheral blood $V\delta2^{+}$ T cells toward a differentiated phenotype. Here, we show that IL-23 signaling and CD26 engagement can contribute to this process.

Both IL-23 (Gerosa et al., 2008) and caveolin-1 (the CD26 ligand; Oyarce et al., 2017; Ohnuma et al., 2004) are expressed by activated dendritic cells (DCs), providing a plausible biological mechanism whereby both IL-23R and CD26 can be engaged on $V\delta2^{+}$ T cells. The impact of IL-23 signaling on $V\delta2^{+}$ T cells has previously been unclear, due in part to reports of disparate effects on adult versus cord blood cells (Moens et al., 2011; Wines et al., 2017), as well as a reported inability of IL-23 to induce STAT3 phosphorylation in freshly isolated or expanded $V\delta2^{+}$ T cells (Wines et al., 2017). Our results provide insight into the observation that IL-23 signaling is substantially more effective in upregulating cytolytic proteins and IL-17 in CBMCs than PBMCs (Moens et al., 2011); given the predominately $CD26^{+}$ phenotype of cord blood $V\delta2^{+}$ T cells compared to many adult donors, the CBMC population should be highly biased toward IL-23 responsiveness. Certain pathogens, such as *Candida albicans* and M*ycobacterium tuberculosis*, are preferential inducers of DC-derived IL-23 (Gerosa et al., 2008; Maher et al., 2015), suggesting that individual variability in $V\delta2^{+}$ differentiation may be influenced by prior infection history and the nature of the innate immune response to infection.

More broadly, our data suggest CD26 surface density is a sensitive marker of $V\delta2^{+}$ T cell phenotype and transcriptional state *ex vivo*, although the expression of CD94/NKG2A modulates $V\delta2^{+}$ T cell functions in response to both cytokine- and TCR-mediated activation. Activation by IL-12/IL-18 stimulation is a feature commonly attributed to $CD161^{+}$ $PLZF^{+}$ T lymphocytes (Fergusson et al., 2014), but it appears that CD26 expression is also tightly linked with this transcriptional program. $V\delta1^{+}$ T cells do not respond to IL-12+IL-18 stimulation, despite quantifiable expression of CD161 (Provine et al., 2018); in contrast, $V\delta1^{+}$ T cells do not express CD26 (not shown), further linking CD26 expression to cytokine responsiveness among unconventional T cells. Whereas CD161 does not functionally contribute to TCR-independent responsiveness (Fergusson et al., 2014), CD26-ADA binding can promote $V\delta2^{+}$ T cell cytokine responsiveness. Importantly, expression of IL-18Rα alone appears to be sub-optimal for the identification of cytokine-reactive T cells, as co-expression of CD26 and CD94 best identified $V\delta2^{+}$ T cells responsive to IL-12/IL-18 stimulation.

There has previously been disparity in the literature regarding the expression of NKG2A and NKG2C on $V\delta1^{+}$ versus $V\delta2^{+}$ T cells, owing in part to inconsistent usage of pan-γδ TCR versus Vδ2-specific reagents (Angelini et al., 2011). In HIV-uninfected individuals, we find that $CD94^{hi}$ cells exclusively co-express NKG2A. Reports have previously indicated that NKG2A signaling can inhibit $V\delta2^{+}$ T cell proliferation or killing in highly activated and expanded $V\delta2^{+}$ T cell lines (Poccia et al., 1997), but we now show that unstimulated $V\delta2^{+}$ T cells are capable of mediating cytotoxicity through CD3 cross-linking and that this is potently inhibited by NKG2A engagement. In contrast, we find no evidence for NKG2C expression on $V\delta2^{+}$ T cells in the majority of adults and were only able to identify a convincing population of CD94/NKG2C-expressing cells in 3 of 51 screened individuals living with HIV. Why HCMV infection is efficient at promoting NKG2C expression on both NK cells and conventional $CD8^{+}$ T cells, but not $V\delta2^{+}$ T cells, remains unknown, particularly considering $V\delta2^{+}$ T cells express several receptors thought to mediate NK cell recognition of cytomegalovirus (CMV)-infected cells, including DNAM-1 (Magri et al., 2011).

Zeb2 expression by $V\delta2^{+}$ T cells is poorly studied, and little is known about the potential target genes regulated by either Zeb2 or Hobit in $V\delta2^{+}$ T cells or how they may co-operate with Tbet and Eomes to determine the cytotoxic activity of $V\delta2^{+}$ T cells. Despite the changes in granzyme expression and cytokine responsiveness between Vδ2 subsets, all CD26/CD94 subsets expressed high levels of PLZF. This suggests that other transcriptional regulators likely play a key role in fine-tuning the transcriptional program typically associated with $PLZF^{+}$ unconventional T cells. Whether the close relationship between *ex vivo* CD26 surface density and transcriptional profile reflects direct regulation of CD26 expression by Zeb2, Hobit, or other transcriptional regulators remains to be determined. Future bulk or single-cell RNA-seq studies with more donors will be informative in understanding the subtle similarities and differences in Vδ2, MAIT cell, and cytotoxic CD8 T cell/NK cell populations.

Phenotypic variation in $V\delta2^{+}$ T cells has implications for both susceptibility to infection and the use of these cells in immunotherapy. $V\delta2^{+}$ T cell IL-23 responsiveness is compromised during active TB infection (Shen et al., 2017) but appears to be a pathway by which $V\delta2^{+}$ T cells can proliferate in Bacillus Calmette-Guerin (BCG)-vaccinated or Mtb-infected animals (Shen et al., 2015). Our results suggest that IL-23-responsive $CD26^{+}$ $V\delta2^{+}$ T cells are lost in a subset of ART-treated, HIV-infected individuals, potentially affecting susceptibility to mycobacterial infection or reactivation. Furthermore, $V\delta2^{+}$ T cells are promising candidates for immunotherapy in part because they can be easily expanded *ex vivo* in the presence of zoledronate/IPP and IL-2 (Berglund et al., 2018; Khan et al., 2014; Roelofs et al., 2009; Kunzmann et al., 1999), and multiple clinical trials have now begun to assess the efficacy of γδ T cell therapy in cancer. Our results suggest, however, that standard expansion of $V\delta2^{+}$ T cell with antigen and IL-2 may be sub-optimal for generating highly cytotoxic cells. The inclusion of IL-23 or other cytokines (or alternately, the selective expansion of specific $V\delta2^{+}$ T cell subsets) to further modify the expression of key transcriptional regulators, such as Hobit; the levels of GzmB; or the expression of negative regulators of cytotoxicity, such as NKG2A, may allow for the further optimization of γδ immunotherapies. Finally, a high concentration of adenosine in tumor microenvironments is a major contributor to the suppression of anti-tumor T cell responses (Antonioli et al., 2013). As a result,

the capacity of CD26 to bind ADA and reduce adenosine-mediated inhibition of T cell function may also provide utility in γδ T-cell-based cancer immunotherapies.

STAR★METHODS

Detailed methods are provided in the online version of this paper and include the following:

- KEY RESOURCES TABLE
- RESOURCE AVAILABILITY
  - Lead Contact
  - Materials Availability
  - Data and Code Availability
- EXPERIMENTAL MODEL AND SUBJECT DETAILS
- METHOD DETAILS
  - Flow cytometry
  - Isolation of γδ T cells
  - RNA sequencing
  - Cell culture and stimulation
  - *In vitro* expansion of Vδ2$^+$ T cells
  - CD3-mediated redirected lysis of P815 cells
- QUANTIFICATION AND STATISTICAL ANALYSIS

SUPPLEMENTAL INFORMATION

Supplemental Information can be found online at https://doi.org/10.1016/j.celrep.2020.107773.

ACKNOWLEDGMENTS

The authors would like to thank the study participants and clinical staff, including Dr. Chantelle Ahlenstiel and Yves d'Udekem and Igor E. Konstantinov from the Department of Cardiac Surgery, Royal Children's Hospital and the BMDI Cord Blood Bank, Murdoch Children's Research Institute. The HIV-infected samples for this project were provided by the Immunovirology Research Network of the Australian Centre for Hepatitis and HIV Virology Research. We acknowledge the Melbourne Cytometry Platform for provision of flow cytometry services and V. Jameson and staff at the Melbourne Brain Centre Flow Cytometry Facility for provision of sorting services. The study was funded by the Australia National Health and Medical Research Council (NHMRC). S.J.K., J.A.J., A.K.W., and D.G.P. are funded by NHMRC fellowships.

AUTHOR CONTRIBUTIONS

Conceptualization, J.A.J., M.S.P., and S.J.K.; Methodology, K.M.W., J.A.J., A.K.W., and S.J.K.; Software, A.K.W. and H.-X.T.; Formal Analysis, K.M.W., J.A.J., H.-X.T., and A.B.K.; Investigation, K.M.W., A.B.K., H.-X.T., and C.V.N.-R.; Resources, A.B.K., S.P.B., D.G.P., C.V.N.-R., and S.J.K.; Data Curation, H.X.T.; Writing – Original Draft, J.A.J.; Writing – Review and Editing, K.M.W., J.A.J., A.K.W., H.-X.T., D.G.P., M.S.P., and S.J.K.; Visualization, K.M.W., J.A.J., A.B.K., A.K.W., and H.-X.T.; Supervision, J.A.J., S.J.K., M.S.P., and D.G.P.; Funding Acquisition, S.J.K.

DECLARATION OF INTERESTS

The authors declare no competing interests.

Received: December 16, 2019
Revised: March 24, 2020
Accepted: May 22, 2020
Published: June 16, 2020

REFERENCES

Abbott, C.A., McCaughan, G.W., Levy, M.T., Church, W.B., and Gorrell, M.D. (1999). Binding to human dipeptidyl peptidase IV by adenosine deaminase and antibodies that inhibit ligand binding involves overlapping, discontinuous sites on a predicted beta propeller domain. Eur. J. Biochem. *266*, 798–810.

Afgan, E., Sloggett, C., Goonasekera, N., Makunin, I., Benson, D., Crowe, M., Gladman, S., Kowsar, Y., Pheasant, M., Horst, R., and Lonie, A. (2015). Genomics virtual laboratory: a practical bioinformatics workbench for the cloud. PLoS ONE *10*, e0140829.

Anders, S., Pyl, P.T., and Huber, W. (2015). HTSeq–a Python framework to work with high-throughput sequencing data. Bioinformatics *31*, 166–169.

Angelini, D.F., Borsellino, G., Poupot, M., Diamantini, A., Poupot, R., Bernardi, G., Poccia, F., Fournié, J.J., and Battistini, L. (2004). FcgammaRIII discriminates between 2 subsets of Vgamma9Vdelta2 effector cells with different responses and activation pathways. Blood *104*, 1801–1807.

Angelini, D.F., Zambello, R., Galandrini, R., Diamantini, A., Placido, R., Micucci, F., Poccia, F., Semenzato, G., Borsellino, G., Santoni, A., and Battistini, L. (2011). NKG2A inhibits NKG2C effector functions of γδ T cells: implications in health and disease. J. Leukoc. Biol. *89*, 75–84.

Antonioli, L., Blandizzi, C., Pacher, P., and Haskó, G. (2013). Immunity, inflammation and cancer: a leading role for adenosine. Nat. Rev. Cancer *13*, 842–857.

Bank, I., and Marcu-Malina, V. (2014). Quantitative peripheral blood perturbations of γδ T cells in human disease and their clinical implications. Clin. Rev. Allergy Immunol. *47*, 311–333.

Berglund, S., Gaballa, A., Sawaisorn, P., Sundberg, B., and Uhlin, M. (2018). Expansion of gammadelta T cells from cord blood: a therapeutical possibility. Stem Cells Int. *2018*, 8529104.

Bolotin, D.A., Poslavsky, S., Mitrophanov, I., Shugay, M., Mamedov, I.Z., Putintseva, E.V., and Chudakov, D.M. (2015). MiXCR: software for comprehensive adaptive immunity profiling. Nat. Methods *12*, 380–381.

Cairo, C., Mancino, G., Cappelli, G., Pauza, C.D., Galli, E., Brunetti, E., and Colizzi, V. (2008). Vdelta2 T-lymphocyte responses in cord blood samples from Italy and Côte d'Ivoire. Immunology *124*, 380–387.

Chen, H., and Boutros, P.C. (2011). VennDiagram: a package for the generation of highly-customizable Venn and Euler diagrams in R. BMC Bioinformatics *12*, 35.

Dang, N.H., Torimoto, Y., Sugita, K., Daley, J.F., Schow, P., Prado, C., Schlossman, S.F., and Morimoto, C. (1990). Cell surface modulation of CD26 by anti-1F7 monoclonal antibody. Analysis of surface expression and human T cell activation. J. Immunol. *145*, 3963–3971.

Davey, M.S., Willcox, C.R., Hunter, S., Kasatskaya, S.A., Remmerswaal, E.B.M., Salim, M., Mohammed, F., Bemelman, F.J., Chudakov, D.M., Oo, Y.H., and Willcox, B.E. (2018). The human Vδ2$^+$ T-cell compartment comprises distinct innate-like Vγ9$^+$ and adaptive Vγ9$^-$ subsets. Nat. Commun. *9*, 1760.

Dias, J., Leeansyah, E., and Sandberg, J.K. (2017). Multiple layers of heterogeneity and subset diversity in human MAIT cell responses to distinct microorganisms and to innate cytokines. Proc. Natl. Acad. Sci. USA *114*, E5434–E5443.

Dimova, T., Brouwer, M., Gosselin, F., Tassignon, J., Leo, O., Donner, C., Marchant, A., and Vermijlen, D. (2015). Effector Vγ9Vδ2 T cells dominate the human fetal γδ T-cell repertoire. Proc. Natl. Acad. Sci. USA *112*, E556–E565.

Dusseaux, M., Martin, E., Serriari, N., Péguillet, I., Premel, V., Louis, D., Milder, M., Le Bourhis, L., Soudais, C., Treiner, E., and Lantz, O. (2011). Human MAIT cells are xenobiotic-resistant, tissue-targeted, CD161hi IL-17-secreting T cells. Blood *117*, 1250–1259.

Fergusson, J.R., Smith, K.E., Fleming, V.M., Rajoriya, N., Newell, E.W., Simmons, R., Marchi, E., Björkander, S., Kang, Y.H., Swadling, L., et al. (2014). CD161 defines a transcriptional and functional phenotype across distinct human T cell lineages. Cell Rep. *9*, 1075–1088.

Gerosa, F., Baldani-Guerra, B., Lyakh, L.A., Batoni, G., Esin, S., Winkler-Pickett, R.T., Consolaro, M.R., De Marchi, M., Giachino, D., Robbiano, A., et al.

(2008). Differential regulation of interleukin 12 and interleukin 23 production in human dendritic cells. J. Exp. Med. *205*, 1447–1461.

Gherardin, N.A., Souter, M.N.T., Koay, H.F., Mangas, K.M., Seemann, T., Stinear, T.P., Eckle, S.B.G., Berzins, S.P., d'Udekem, Y., Konstantinov, I.E., et al. (2018). Human blood MAIT cell subsets defined using MR1 tetramers. Immunol. Cell Biol. *96*, 507–525.

Godfrey, D.I., Uldrich, A.P., McCluskey, J., Rossjohn, J., and Moody, D.B. (2015). The burgeoning family of unconventional T cells. Nat. Immunol. *16*, 1114–1123.

Gu, Z., Gu, L., Eils, R., Schlesner, M., and Brors, B. (2014). circlize Implements and enhances circular visualization in R. Bioinformatics *30*, 2811–2812.

Gumá, M., Angulo, A., Vilches, C., Gómez-Lozano, N., Malats, N., and López-Botet, M. (2004). Imprint of human cytomegalovirus infection on the NK cell receptor repertoire. Blood *104*, 3664–3671.

Gumá, M., Budt, M., Sáez, A., Brckalo, T., Hengel, H., Angulo, A., and López-Botet, M. (2006). Expansion of CD94/NKG2C+ NK cells in response to human cytomegalovirus-infected fibroblasts. Blood *107*, 3624–3631.

Gutierrez-Arcelus, M., Teslovich, N., Mola, A.R., Polidoro, R.B., Nathan, A., Kim, H., Hannes, S., Slowikowski, K., Watts, G.F.M., Korsunsky, I., et al. (2019). Lymphocyte innateness defined by transcriptional states reflects a balance between proliferation and effector functions. Nat. Commun. *10*, 687.

Harly, C., Guillaume, Y., Nedellec, S., Peigné, C.M., Mönkkönen, H., Mönkkönen, J., Li, J., Kuball, J., Adams, E.J., Netzer, S., et al. (2012). Key implication of CD277/butyrophilin-3 (BTN3A) in cellular stress sensing by a major human γδ T-cell subset. Blood *120*, 2269–2279.

Hatano, R., Yamada, T., Matsuoka, S., Iwata, S., Yamazaki, H., Komiya, E., Okamoto, T., Dang, N.H., Ohnuma, K., and Morimoto, C. (2014). Establishment of monoclonal anti-human CD26 antibodies suitable for immunostaining of formalin-fixed tissue. Diagn. Pathol. *9*, 30.

Hinks, T.S.C., Marchi, E., Jabeen, M., Olshansky, M., Kurioka, A., Pediongco, T.J., Meehan, B.S., Kostenko, L., Turner, S.J., Corbett, A.J., et al. (2019). Activation and in vivo evolution of the MAIT cell transcriptome in mice and humans reveals tissue repair functionality. Cell Rep. *28*, 3249–3262.e5.

Hoeres, T., Smetak, M., Pretscher, D., and Wilhelm, M. (2018). Improving the efficiency of Vγ9Vδ2 T-cell immunotherapy in cancer. Front. Immunol. *9*, 800.

Jagannathan, P., Lutwama, F., Boyle, M.J., Nankya, F., Farrington, L.A., McIntyre, T.I., Bowen, K., Naluwu, K., Nalubega, M., Musinguzi, K., et al. (2017). Vδ2+ T cell response to malaria correlates with protection from infection but is attenuated with repeated exposure. Sci. Rep. *7*, 11487.

Juno, J.A., and Eriksson, E.M. (2019). γδ T-cell responses during HIV infection and antiretroviral therapy. Clin. Transl. Immunology *8*, e01069.

Juno, J.A., Waruk, J.L.M., Harris, A., Mesa, C., Lopez, C., Bueti, J., Ball, T.B., and Kiazyk, S.A. (2017). γδ T-cell function is inhibited in end-stage renal disease and impacted by latent tuberculosis infection. Kidney Int. *92*, 1003–1014.

Kameoka, J., Tanaka, T., Nojima, Y., Schlossman, S.F., and Morimoto, C. (1993). Direct association of adenosine deaminase with a T cell activation antigen, CD26. Science *261*, 466–469.

Khan, M.W., Curbishley, S.M., Chen, H.C., Thomas, A.D., Pircher, H., Mavilio, D., Steven, N.M., Eberl, M., and Moser, B. (2014). Expanded human blood-derived γδT cells display potent antigen-presentation functions. Front. Immunol. *5*, 344.

Kim, D., Langmead, B., and Salzberg, S.L. (2015). HISAT: a fast spliced aligner with low memory requirements. Nat. Methods *12*, 357–360.

Koay, H.F., Gherardin, N.A., Xu, C., Seneviratna, R., Zhao, Z., Chen, Z., Fairlie, D.P., McCluskey, J., Pellicci, D.G., Uldrich, A.P., and Godfrey, D.I. (2019). Diverse MR1-restricted T cells in mice and humans. Nat. Commun. *10*, 2243.

Kondo, M., Izumi, T., Fujieda, N., Kondo, A., Morishita, T., Matsushita, H., and Kakimi, K. (2011). Expansion of human peripheral blood γδ T cells using zoledronate. J. Vis. Exp. (*55*), 3182.

Kunzmann, V., Bauer, E., and Wilhelm, M. (1999). Gamma/delta T-cell stimulation by pamidronate. N. Engl. J. Med. *340*, 737–738.

Kurioka, A., Ussher, J.E., Cosgrove, C., Clough, C., Fergusson, J.R., Smith, K., Kang, Y.H., Walker, L.J., Hansen, T.H., Willberg, C.B., and Klenerman, P. (2015). MAIT cells are licensed through granzyme exchange to kill bacterially sensitized targets. Mucosal Immunol. *8*, 429–440.

Lawand, M., Déchanet-Merville, J., and Dieu-Nosjean, M.C. (2017). Key features of gamma-delta T-cell subsets in human diseases and their immunotherapeutic implications. Front. Immunol. *8*, 761.

Lazetic, S., Chang, C., Houchins, J.P., Lanier, L.L., and Phillips, J.H. (1996). Human natural killer cell receptors involved in MHC class I recognition are disulfide-linked heterodimers of CD94 and NKG2 subunits. J. Immunol. *157*, 4741–4745.

Le Nours, J., Gherardin, N.A., Ramarathinam, S.H., Awad, W., Wiede, F., Gully, B.S., Khandokar, Y., Praveena, T., Wubben, J.M., Sandow, J.J., et al. (2019). A class of γδ T cell receptors recognize the underside of the antigen-presenting molecule MR1. Science *366*, 1522–1527.

Leeansyah, E., Svärd, J., Dias, J., Buggert, M., Nyström, J., Quigley, M.F., Moll, M., Sönnerborg, A., Nowak, P., and Sandberg, J.K. (2015). Arming of MAIT cell cytolytic antimicrobial activity is induced by IL-7 and defective in HIV-1 infection. PLoS Pathog. *11*, e1005072.

Li, H., Chaudhry, S., Poonia, B., Shao, Y., and Pauza, C.D. (2013). Depletion and dysfunction of Vγ2Vδ2 T cells in HIV disease: mechanisms, impacts and therapeutic implications. Cell. Mol. Immunol. *10*, 42–49.

Magri, G., Muntasell, A., Romo, N., Sáez-Borderías, A., Pende, D., Geraghty, D.E., Hengel, H., Angulo, A., Moretta, A., and López-Botet, M. (2011). NKp46 and DNAM-1 NK-cell receptors drive the response to human cytomegalovirus-infected myeloid dendritic cells overcoming viral immune evasion strategies. Blood *117*, 848–856.

Maher, C.O., Dunne, K., Comerford, R., O'Dea, S., Loy, A., Woo, J., Rogers, T.R., Mulcahy, F., Dunne, P.J., and Doherty, D.G. (2015). Candida albicans stimulates IL-23 release by human dendritic cells and downstream IL-17 secretion by Vδ1 T cells. J. Immunol. *194*, 5953–5960.

Mela, C.M., and Goodier, M.R. (2007). The contribution of cytomegalovirus to changes in NK cell receptor expression in HIV-1-infected individuals. J. Infect. Dis. *195*, 158–159, author reply 159–160.

Mela, C.M., Burton, C.T., Imami, N., Nelson, M., Steel, A., Gazzard, B.G., Gotch, F.M., and Goodier, M.R. (2005). Switch from inhibitory to activating NKG2 receptor expression in HIV-1 infection: lack of reversion with highly active antiretroviral therapy. AIDS *19*, 1761–1769.

Moens, E., Brouwer, M., Dimova, T., Goldman, M., Willems, F., and Vermijlen, D. (2011). IL-23R and TCR signaling drives the generation of neonatal Vgamma9Vdelta2 T cells expressing high levels of cytotoxic mediators and producing IFN-gamma and IL-17. J. Leukoc. Biol. *89*, 743–752.

Ohnuma, K., Yamochi, T., Uchiyama, M., Nishibashi, K., Yoshikawa, N., Shimizu, N., Iwata, S., Tanaka, H., Dang, N.H., and Morimoto, C. (2004). CD26 up-regulates expression of CD86 on antigen-presenting cells by means of caveolin-1. Proc. Natl. Acad. Sci. USA *101*, 14186–14191.

Ohnuma, K., Uchiyama, M., Yamochi, T., Nishibashi, K., Hosono, O., Takahashi, N., Kina, S., Tanaka, H., Lin, X., Dang, N.H., and Morimoto, C. (2007). Caveolin-1 triggers T-cell activation via CD26 in association with CARMA1. J. Biol. Chem. *282*, 10117–10131.

Oyarce, C., Cruz-Gomez, S., Galvez-Cancino, F., Vargas, P., Moreau, H.D., Diaz-Valdivia, N., Diaz, J., Salazar-Onfray, F.A., Pacheco, R., Lennon-Dumenil, A.M., et al. (2017). Caveolin-1 expression increases upon maturation in dendritic cells and promotes their migration to lymph nodes thereby favoring the induction of $CD8^+$ T cell responses. Front. Immunol. *8*, 1794.

Pauza, C.D., Liou, M.L., Lahusen, T., Xiao, L., Lapidus, R.G., Cairo, C., and Li, H. (2018). Gamma delta T cell therapy for cancer: it is good to be local. Front. Immunol. *9*, 1305.

Poccia, F., Cipriani, B., Vendetti, S., Colizzi, V., Poquet, Y., Battistini, L., López-Botet, M., Fournié, J.J., and Gougeon, M.L. (1997). CD94/NKG2 inhibitory receptor complex modulates both anti-viral and anti-tumoral responses of polyclonal phosphoantigen-reactive V gamma 9V delta 2 T lymphocytes. J. Immunol. *159*, 6009–6017.

Provine, N.M., Binder, B., FitzPatrick, M.E.B., Schuch, A., Garner, L.C., Williamson, K.D., van Wilgenburg, B., Thimme, R., Klenerman, P., and Hofmann, M. (2018). Unique and common features of innate-like human Vδ2^{+} γδT cells and mucosal-associated invariant T cells. Front. Immunol. *9*, 756.

Qaqish, A., Huang, D., Chen, C.Y., Zhang, Z., Wang, R., Li, S., Yang, E., Lu, Y., Larsen, M.H., Jacobs, W.R., Jr., et al. (2017). Adoptive transfer of phosphoantigen-specific γδ T cell subset attenuates *Mycobacterium tuberculosis* infection in nonhuman primates. J. Immunol. *198*, 4753–4763.

Roelofs, A.J., Jauhiainen, M., Mönkkönen, H., Rogers, M.J., Mönkkönen, J., and Thompson, K. (2009). Peripheral blood monocytes are responsible for gammadelta T cell activation induced by zoledronic acid through accumulation of IPP/DMAPP. Br. J. Haematol. *144*, 245–250.

Ryan, P.L., Sumaria, N., Holland, C.J., Bradford, C.M., Izotova, N., Grandjean, C.L., Jawad, A.S., Bergmeier, L.A., and Pennington, D.J. (2016). Heterogeneous yet stable Vδ2(+) T-cell profiles define distinct cytotoxic effector potentials in healthy human individuals. Proc. Natl. Acad. Sci. USA *113*, 14378–14383.

Sharma, P.K., Wong, E.B., Napier, R.J., Bishai, W.R., Ndung'u, T., Kasprowicz, V.O., Lewinsohn, D.A., Lewinsohn, D.M., and Gold, M.C. (2015). High expression of CD26 accurately identifies human bacteria-reactive MR1-restricted MAIT cells. Immunology *145*, 443–453.

Shen, H., Wang, Y., Chen, C.Y., Frencher, J., Huang, D., Yang, E., Ryan-Payseur, B., and Chen, Z.W. (2015). Th17-related cytokines contribute to recall-like expansion/effector function of HMBPP-specific Vγ2Vδ2 T cells after Mycobacterium tuberculosis infection or vaccination. Eur. J. Immunol. *45*, 442–451.

Shen, H., Gu, J., Xiao, H., Liang, S., Yang, E., Yang, R., Huang, D., Chen, C., Wang, F., Shen, L., and Chen, Z.W. (2017). Selective destruction of interleukin-23 induced expansion of a major antigen-specific γδ T-cell subset in patients with tuberculosis. J. Infect. Dis. *215*, 420–430.

Shugay, M., Bagaev, D.V., Turchaninova, M.A., Bolotin, D.A., Britanova, O.V., Putintseva, E.V., Pogorelyy, M.V., Nazarov, V.I., Zvyagin, I.V., Kirgizova, V.I., et al. (2015). VDJtools: unifying post-analysis of T cell receptor repertoires. PLoS Comput. Biol. *11*, e1004503.

Ussher, J.E., Bilton, M., Attwod, E., Shadwell, J., Richardson, R., de Lara, C., Mettke, E., Kurioka, A., Hansen, T.H., Klenerman, P., and Willberg, C.B. (2014). CD161++ CD8+ T cells, including the MAIT cell subset, are specifically activated by IL-12+IL-18 in a TCR-independent manner. Eur. J. Immunol. *44*, 195–203.

van Helden, M.J., Goossens, S., Daussy, C., Mathieu, A.L., Faure, F., Marçais, A., Vandamme, N., Farla, N., Mayol, K., Viel, S., et al. (2015). Terminal NK cell maturation is controlled by concerted actions of T-bet and Zeb2 and is essential for melanoma rejection. J. Exp. Med. *212*, 2015–2025.

Wang, H., Kjer-Nielsen, L., Shi, M., D'Souza, C., Pediongco, T.J., Cao, H., Kostenko, L., Lim, X.Y., Eckle, S.B.G., Meehan, B.S., et al. (2019). IL-23 costimulates antigen-specific MAIT cell activation and enables vaccination against bacterial infection. Sci. Immunol. *4*, eaaw0402.

Wines, B.D., Yap, M.L., Powell, M.S., Tan, P.S., Ko, K.K., Orlowski, E., and Hogarth, P.M. (2017). Distinctive expression of interleukin-23 receptor subunits on human Th17 and γδ T cells. Immunol. Cell Biol. *95*, 272–279.

Yu, J., Mao, H.C., Wei, M., Hughes, T., Zhang, J., Park, I.K., Liu, S., McClory, S., Marcucci, G., Trotta, R., and Caligiuri, M.A. (2010). CD94 surface density identifies a functional intermediary between the CD56bright and CD56dim human NK-cell subsets. Blood *115*, 274–281.

Zhao, Y., Niu, C., and Cui, J. (2018). Gamma-delta (γδ) T cells: friend or foe in cancer development? J. Transl. Med. *16*, 3.

STAR★METHODS

KEY RESOURCES TABLE

REAGENT or RESOURCE	SOURCE	IDENTIFIER
Antibodies		
Rat monoclonal anti-CCR5 APC conjugated (clone: J418F1)	BioLegend	Cat# 359122; RRID: AB_2564073
Rat monoclonal anti-CCR5 BV421 conjugated (clone: J418F1)	BioLegend	Cat# 359118; RRID: AB_2563577
Mouse monoclonal anti-CCR6 BV785 conjugated (clone: G034E3)	BioLegend	Cat# 353422; RRID: AB_2563660
Mouse monoclonal anti-CCR6 BV785 conjugated (clone: 11A9)	BD Biosciences	Cat# 560620; RRID: AB_1727440
Mouse monoclonal anti-CD3 APC-H7 conjugated (clone: SK7)	BD Biosciences	Cat# 560176; RRID: AB_1645475
Mouse monoclonal anti-CD3 BV510 conjugated (clone: SK7)	BioLegend	Cat# 344828; RRID: AB_2563704
Mouse monoclonal anti-CD3 BV510 conjugated (clone: SK7)	BioLegend	Cat# 344842; RRID: AB_2616891
Mouse monoclonal anti-CD3 BUV805 conjugated (clone: SK7)	BD Biosciences	Cat# 612893
Mouse monoclonal anti-CD3 Alexa Fluor 700 conjugated (clone: SP34-2)	BD Biosciences	Cat# 557917; RRID: AB_396938
Mouse monoclonal anti-CD3 unconjugated (clone: OKT3)	Thermo Fisher Scientific	Cat# 16-0037-85; RRID: AB_468855
Mouse monoclonal anti-CD8a BV650 conjugated (clone: RPA-T8)	BioLegend	Cat# 301042; RRID: AB_2563505
Mouse monoclonal anti-CD16 Alexa Fluor 700 conjugated (clone: 3G8)	BD Biosciences	Cat# 560713; RRID: AB_1727430
Mouse monoclonal anti-CD16 BV605 conjugated (clone: 3G8)	BD Biosciences	Cat# 563172; RRID: AB_2744297
Mouse monoclonal anti-CD16 BV650 conjugated (clone: 3G8)	BD Biosciences	Cat# 563691; RRID: AB_2744298
Mouse monoclonal anti-CD26 FITC conjugated (clone: BA5b)	BioLegend	Cat# 302704; RRID: AB_314288
Mouse monoclonal anti-CD26 APC conjugated (clone: BA5b)	BioLegend	Cat# 302710; RRID: AB_10916120
Mouse monoclonal anti-CD26 unconjugated (clone: 1F7)	Dr. Chikao Morimoto, NIH AIDS Reagent Program	Cat# 2462
Mouse monoclonal anti-CD26 unconjugated (clone: 5F8)	Dr. Chikao Morimoto, NIH AIDS Reagent Program	Cat# 2463
Mouse monoclonal anti-CD27 BV510 conjugated (clone: M-T271)	BioLegend	Cat# 356420; RRID: AB_2562603
Mouse monoclonal anti-CD27 BV650 conjugated (clone: O323)	BioLegend	Cat# 302828; RRID: AB_2562096
Mouse monoclonal anti-CD27 BUV737 conjugated (clone: L128)	BD Biosciences	Cat# 612829
Mouse monoclonal anti-CD28 BV711 conjugated (clone: CD28.2)	BD Biosciences	Cat# 563131; RRID: AB_2738020
Mouse monoclonal anti-CD45RA FITC conjugated (clone: HI100)	BioLegend	Cat# 304106; RRID: AB_314410

(*Continued on next page*)

Continued

REAGENT or RESOURCE	SOURCE	IDENTIFIER
Mouse monoclonal anti-CD45RA PerCP-Cy5.5 conjugated (clone: HI100)	BioLegend	Cat# 304122; RRID: AB_893357
Mouse monoclonal anti-CD45RA PE-Cy7 conjugated (clone: HI100)	BD Biosciences	Cat# 560675; RRID: AB_1727498
Mouse monoclonal anti-CD56 BUV395 conjugated (clone: NCAM16.2)	BD Biosciences	Cat# 563554; RRID: AB_2687886
Mouse monoclonal anti-CD56 BUV737 conjugated (clone: NCAM16.2)	BD Biosciences	Cat# 564447; RRID: AB_2744432
Mouse monoclonal anti-CD57 Pacific Blue conjugated (clone: HCD57)	BioLegend	Cat# 322316; RRID: AB_2063197
Mouse monoclonal anti-CD57 BV510 conjugated (clone: QA17A04)	BioLegend	Cat# 393313; RRID: AB_2750341
Mouse monoclonal anti-CD94 APC conjugated (clone: HP-3D9)	BD Biosciences	Cat# 559876; RRID: AB_398679
Mouse monoclonal anti-CD94 APC conjugated (clone: HP-3D9)	BD Biosciences	Cat# 743954; RRID: AB_2741876
Mouse monoclonal anti-CD127 APC-Alexa Fluor 700 conjugated (clone: R34.34)	Beckman Coulter	Cat# A71116
Mouse monoclonal anti-CD161 BV421 conjugated (clone: HP-3G10)	BioLegend	Cat# 339914, RRID:AB_2561421
Rat monoclonal anti-CX3CR1 FITC conjugated (clone: 2A9-1)	BioLegend	Cat# 341606; RRID: AB_1626272
Rat monoclonal anti-CX3CR1 PE-Cy7 conjugated (clone: 2A9-1)	BioLegend	Cat# 341612; RRID: AB_10900816
Mouse monoclonal anti-DNAM-1 BV605 conjugated (clone: 11A8)	BioLegend	Cat# 338324; RRID: AB_2721543
Mouse monoclonal anti-DNAM-1 PE conjugated (clone: 11A8)	BioLegend	Cat# 338306; RRID: AB_2275498
Mouse monoclonal anti-EOMES PE-eFluor 610 conjugated (clone: WD1928)	Thermo Fisher Scientific	Cat# 61-4877-42; RRID: AB_2574616
Mouse monoclonal anti-Granzyme B BV510 conjugated (clone: GB11)	BD Biosciences	Cat# 563388; RRID: AB_2738174
Mouse monoclonal anti-Granzyme B BV510 conjugated (clone: GB11)	BD Biosciences	Cat# 563388; RRID: AB_2738174
Mouse monoclonal anti-Granzyme K PerCP-Cy5.5 conjugated (clone: GM26E7)	BioLegend	Cat# 370514; RRID: AB_2632852
Armenian hamster monoclonal anti-Helios PE Dazzle 594 conjugated (clone: 22F6)	BioLegend	Cat# 137231; RRID: AB_2565796
Mouse monoclonal anti-Hobit Alexa 647 conjugated (clone: Sanquin-Hobit/1)	BD Biosciences	Cat# 566250; RRID: AB_2739629
Mouse monoclonal anti-IFNγ APC conjugated (clone: B27)	BioLegend	Cat# 506510; RRID: AB_315443
Mouse monoclonal anti-IFNγ BUV395 conjugated (clone: B27)	BD Biosciences	Cat# 563563; RRID:AB_2738277
Mouse monoclonal anti-IL-18Rα APC conjugated (clone: H44)	Miltenyi Biotec	Cat# 130-101-728; RRID: AB_2656350
Mouse monoclonal anti-IL-18Rα PE-Vio770 conjugated (clone: H44)	Miltenyi Biotec	Cat# 130-101-723; RRID: AB_2656352
Mouse IgG1, κ Isotype control antibody (clone: MOPC-21)	BioLegend	Cat# 400153
Mouse monoclonal anti-NKG2A APC conjugated (clone: Z199)	Beckman Coulter	Cat# A60797; RRID: AB_10643105

(*Continued on next page*)

Continued

REAGENT or RESOURCE	SOURCE	IDENTIFIER
Mouse monoclonal anti-NKG2A unconjugated (clone: Z199)	Beckman Coulter	Cat# IM2750; RRID:AB_131495
Mouse monoclonal anti-NKG2C PE conjugated (clone: 134591)	R and D Systems	Cat# FAB138P; RRID: AB_2132983
Mouse monoclonal anti-PLZF Alexa Fluor 647 conjugated (clone: R17-809)	BD Biosciences	Cat# 563490; RRID: AB_2738238
Mouse monoclonal anti-RORγT PE conjugated (clone: Q21-559)	BD Biosciences	Cat# 563081; RRID: AB_2686896
Mouse monoclonal anti-Tbet BV421 conjugated (clone: 4B10)	BioLegend	Cat# 644816; RRID: AB_10959653
Mouse monoclonal anti-Tbet BV786 conjugated (clone: O4-46)	BD Biosciences	Cat# 564141; RRID: AB_2738615
Mouse monoclonal anti-TNFα Alexa Fluor 700 conjugated (clone: MAb11)	BD Biosciences	Cat# 557996; RRID: AB_396978
Mouse monoclonal anti-TNFα APC-Cy7 conjugated (clone: MAb11)	BioLegend	Cat# 502944, RRID: AB_2562870
Mouse monoclonal anti-Vα7.2 BV510 conjugated (clone: 3C10)	BioLegend	Cat# 351717; RRID: AB_2562535
Mouse monoclonal anti-Vδ1 FITC conjugated (clone: TS8.2)	Thermo Fisher Scientific	Cat# TCR2730; RRID: AB_22362
Mouse monoclonal anti-Vγ9 PE conjugated (clone: B3)	BioLegend	Cat# 331308; RRID: AB_1236408
Mouse monoclonal anti-Vδ2 FITC conjugated (clone: B6)	BioLegend	Cat# 331406; RRID: AB_1089230
Mouse monoclonal anti-Vδ2 BV786 conjugated (clone: B6)	BD Biosciences	Cat# 743753; RRID: AB_2741721
Mouse monoclonal anti-Vδ2 PE conjugated (clone: B6)	BioLegend	Cat# 331408; RRID: AB_1089232
Mouse monoclonal anti-Vδ2 FITC conjugated (clone: 15D)	Thermo Fisher Scientific	Cat# TCR2732, RRID: AB_417095
Biological Samples		
Healthy human whole blood	University of Melbourne Department of Microbiology and Immunology; Australian Red Cross Service; Royal Children's Hospital Melbourne	N/A
Human cord blood	BMDI Cord Blood Bank, Murdoch Children's Research Institute	N/A
PBMC from HIV-1 infected humans	Melbourne Sexual Health Clinic; Immnovirology Research Network, Australian Centre for Hepatitis and HIV Virology Research	N/A
Chemicals, Peptides, and Recombinant Proteins		
Recombinant human IL-12	InVivogen	Cat# rcyc-hil12; Accession #P29459
Recombinant human IL-18	InVivogen	Cat# rcyec-hil18; Accession #Q14116
Recombinant human IL-23	R and D Systems	Cat# 1290-IL; Accession #P29460
Recombinant human IL-7	Thermo Fisher Scientific	Cat# 14-8079-62
Recombinant human IL-2	Peprotech	Cat# 200-02; Accession #P60568
Adenosine deaminase from bovine intestine	Sigma Aldrich	Cat# 10102105001
Zoledronic acid monohydrate	Sigma Aldrich	Cat# SML0223; CAS# 165800-06-6
Live/dead fixable blue dead cell stain	Thermo Fisher Scientific	Cat# L23105
Cytofix	BD Biosciences	Cat# 554655
Cytofix/cytoperm kit	BD Biosciences	Cat# 554714

(*Continued on next page*)

Continued

REAGENT or RESOURCE	SOURCE	IDENTIFIER
Transcription buffer staining kit	BD Biosciences	Cat# 562574
(*E*)-1-Hydroxy-2-methyl-2-butenyl 4-pyrophosphate lithium salt	Sigma Aldrich	Cat# 95098; CAS# 396726-03-7
Human MR1 5-OP-RU tetramer	Dr. James McCluskey University of Melbourne	
Streptavidin-BV421	BioLegend	Cat# 405225
Streptavidin-PE	BioLegend	Cat# 405203
GolgiStop	BD Biosciences	Cat# 554724
GolgiPlug	BD Biosciences	Cat# 555029
Sitagliptin phosphate monohydrate	Santa Cruz Biotechnology	Cat# SCZSC-364620; CAS# 654671-77-9
P32/98	Santa Cruz Biotechnology	Cat# SCZSC-201305; CAS# 136259-20-6
Critical Commercial Assays		
PrimeFlow RNA assay kit	Thermo Fisher Scientific	Cat# 88-18005-210
TCRγ/δ^+ T Cell Isolation Kit, human	MACS Miltenyi Biotec	Cat# 130-092-892
Anti-TCRγ/δ MicroBead Kit, human	MACS Miltenyi Biotec	Cat# 130-050-701
miRNeasy® Plus Micro Kit	QIAGEN	Cat# 217084
TruSeq® Stranded mRNA Library Prep	Illumina	Cat# 20020594
CytoTox 96® Non-Radioactive Cytotoxicity Assay	Promega	Cat# G1780
Deposited Data		
Raw sequence reads	This paper	GEO: GSE122409
Experimental Models: Cell Lines		
P815 cells	ATCC	TIB-64
Oligonucleotides		
PrimeFlow Gene Probes - DapB	ThermoFisher Scientific	Assay ID VF1-11712-PF
PrimeFlow Gene Probes - RPL13A	ThermoFisher Scientific	Assay ID VA4-13187-PF
PrimeFlow Gene Probes - Zeb2	ThermoFisher Scientific	Assay ID VA1-16233-PF
Software and Algorithms		
FlowJo v10.2	TreeStar	https://www.flowjo.com/
Galaxy	Melbourne Bioinformatics	https://usegalaxy.org/
HTSeq	Anders et al., 2015	https://htseq.readthedocs.io/en/master/#
Degust	Powell https://doi.org/10.5281/zenodo.3258932.	http://degust.erc.monash.edu
MIXCR	Bolotin et al., 2015	https://mixcr.readthedocs.io/en/master/
VDJtools	Shugay et al., 2015	https://vdjtools-doc.readthedocs.io/en/master/
circlize	Gu et al., 2014	https://jokergoo.github.io/circlize_book/book/
VennDiagram	Chen and Boutros, 2011	https://cran.r-project.org/web/packages/VennDiagram/VennDiagram.pdf
Morpheus	The Broad Institute	https://software.broadinstitute.org/morpheus/
Prism 7	GraphPad	https://www.graphpad.com/scientific-software/prism/

RESOURCE AVAILABILITY

Lead Contact

Further information and requests for resources and reagents should be directed to and will be fulfilled by the Lead Contact, Jennifer Juno (jennifer.juno@unimelb.edu.au).

Materials Availability

This study did not generate new unique reagents.

Data and Code Availability

The RNaseq datasets generated during this study are available at the Gene Expression Omnibus under code GSE122409. Transcriptomic data for MAIT and CD8 populations were obtained from a previously published dataset under code GEO: 123805.

EXPERIMENTAL MODEL AND SUBJECT DETAILS

Whole blood samples were collected from 32 healthy donors, recruited at the University of Melbourne or provided by the Australian Red Cross Service and the Royal Children's Hospital. Donors from the University of Melbourne included both men and women, but no demographic information was available for donors recruited through the Australian Red Cross. Cord blood samples were provided by the BMDI Cord Blood Bank, Murdoch Children's Research Institute. Peripheral blood mononuclear cells (PBMC) were isolated by Ficoll density gradient centrifugation and washed in RPMI supplemented with 10% fetal calf serum (FCS, Sigma) and penicillin/streptomycin/L-glutamate (RF10) prior to use or cryopreservation in liquid nitrogen for future analysis. A subset of 15 donors was screened for HCMV seropositivity by the Victorian Infectious Disease Reference Laboratory (VIDRL). Cryopreserved PBMC samples from 24 HIV-1 infected participants were obtained from the Immunovirology Research Network (IVRN) of the Australian Centre for Hepatitis and HIV Virology Research (ACH^2). The characteristics of this cohort are reported in Table S2. An additional cohort of cryopreserved PBMC (n = 27) from the Melbourne Sexual Health Clinic (MSHC) collected for previous studies were screened for NKG2C expression. All subjects provided informed consent prior to the collection of samples, and all procedures were conducted with the approval of the relevant Institute's ethics committee.

METHOD DETAILS

Flow cytometry

To characterize lymphocyte phenotypes, 2.0 × 10^6 thawed or freshly isolated PBMC were washed and stained with viability dye (Live/Dead fixable dead cell stain, Life Technologies) followed by a cocktail of antibodies for 30 min at 4°C. Cells were then washed and fixed with BD Cytofix (BD Biosciences). Cytokine and transcription factor expression was assessed by intracellular antibody staining following permeabilization with BD Cytofix/Cytoperm or BD Transcription Staining Buffer (BD Biosciences), respectively.

Isolation of γδ T cells

γδ T cells were negatively selected from freshly isolated PBMC using the human TCR γδ T Cell Isolation Kit (Miltenyi Biotec) according to the manufacturer's instructions. In some experiments, due to the timing of blood collection, freshly isolated PBMC were cultured for 18 hours in RF10 prior to γδ T cell isolation. For some experiments, Vδ2$^+$ cells were isolated by cell sorting. For sorting, cells were surface stained, washed and resuspended in PBS + 2% FCS. Sorting was performed on a BD ARIA III (BD Biosciences) at the Melbourne Brain Centre, University of Melbourne and sorted cells were collected into FCS or RNA lysis buffer (RLT buffer).

RNA sequencing

For the *ex vivo* RNA sequencing data, freshly isolated PBMC from three healthy donors were stained for CD3, Vδ2 TCR, CD26 and CD94. Cells were identified as Live/Dead negative, CD3$^+$ Vδ2$^+$ cells. Four populations (CD26$^+$CD94^{lo}, CD26$^+$CD94^{hi}, CD26$^-$CD94^{hi}, CD26$^-$CD94^{lo}) were sorted into RLT buffer (QIAGEN) containing 0.14M β-mercaptoethanol (Sigma). Post-sort, cells were suspended in a volume of RLT buffer representing 3.5x the sorting solution volume. Genomic DNA was removed using a gDNA eliminator (QIAGEN), according the manufacturer's protocol. RNA was extracted by addition of 100% ethanol in a 5:7 volume ratio to flow-through solution and processed with the RNeasy Plus Micro Kit (QIAGEN), according to the manufacturer's instructions.

For the Vδ2$^+$ *in vitro* expansion RNA sequencing, individual CD26/CD94 Vδ2 subsets were sorted from a single blood draw and expanded in parallel with γδ-depleted PBMC, zoledronate, IL-2 and (if applicable) IL-23. At day 14 post-stimulation, cells were surface stained and live, CD3$^+$ Vδ2$^+$ cells were sorted, pelleted and frozen at −80°C. RNA was isolated from sorted cells using the Direct-zol RNA MicroPrep Kit (Zymo), as per manufacturer's protocol.

The Australian Genome Research Facility (Melbourne, Australia) performed the RNaseq with an Illumina HiSeq 2500 or NovaSeq 6000, and obtained 100bp single reads. The library was prepared with a TruSeq Stranded mRNA Library Prep Kit (Illumina).

Cell culture and stimulation

Unless otherwise noted, all experiments were performed on primary human PBMC or Vδ2$^+$ T cells. If cryopreserved, PBMC samples were thawed, washed and counted. Bulk PBMC were cultured in RF10 at 2x10^6/mL and stimulated with 50ng/ml IL-12 and IL-18 for 24 hours with the addition of Golgi Stop and Golgi Plug (BD Biosciences) after 8 hours. In some experiments, 1 – 8IU/ml of ADA was added to the cell culture during stimulation with IL-12 and IL-18. Where indicated, cells were preincubated with a 1:250 dilution of anti-CD26 5F8 ascites (corresponding to approximately 15 μg /mL) or isotype control (MOPC-21, Biolegend) for 45 minutes at

37°C prior to cytokine and ADA stimulation. Alternatively, 0.1 – 10μg/ml of Sitagliptin (Santa Cruz Biotechnology) or 0.1 – 5μg/ml P32 (Santa Cruz Biotechnology) were included in the IL-12/IL-18 stimulations.

For antigen stimulations, cells were stimulated with 20ng/ml HMB-PP for 16 hours with Golgi Stop and Golgi Plug added 1 hr post-stimulation. In some cases, PBMC were stimulated with 50ng/ml recombinant human IL-23 for 18 hours. For stimulation of isolated or sorted γδ T cells, 0.2x10^5 to 1x10^5 cells were seeded in RF10 in a 96-well plate. Cells were stimulated with 50ng/ml IL-7 (Life Technologies) with or without 50ng/ml IL-23 for 5 days.

To determine the impact of CD26 ligation on CD26 surface expression, bulk PBMC were stimulated with anti-CD26 monoclonal antibodies 1F7 (1:500 dilution) or 5F8 (1:1250 dilution) corresponding to approximately 3μg/mL, or an isotype control (MOPC-21) for 1 hour at 37°C and washed 3 times. Cells were then cultured for 3 days in RF10 at 2x10^6/mL.

In vitro expansion of Vδ2$^+$ T cells

Freshly isolated PBMC from a single blood draw were divided into two aliquots: one for γδ T cell depletion, and one for γδ T cell isolation. γδ T cells were depleted using the γδ T cell Microbead Kit (Miltenyi) according to the manufacturer's instructions. γδ T cell were isolated using the γδ T cell isolation kit (Miltenyi) according to the manufacturer's instructions. Unlabelled γδ T cells were collected and stained with Vδ1 TCR, CD26 and CD94 antibodies. Cells were then sorted on a BD FACS Aria II sorter, and Vδ1$^-$ CD26^{hi}CD94^{lo}, CD26$^+$CD94hi, CD26$^-$CD94^{hi} and CD26$^-$CD94^{lo} populations were collected. 50-200x10^5 sorted cells (depending on the donor, but consistent between subsets) were added back into γδ T cell-depleted PBMC. Expansion of Vδ2$^+$ T cells was performed in a protocol similar to Kondo et al. (2011), with γδ/PBMC cultures stimulated for 14 days with 15μM Zoledronate and 100IU/ml IL-2. In some experiments, cultures were divided into two aliquots, one of which was additionally cultured with 50ng/ml of IL-23 beginning on day 0. Media was replaced every 3-4 days (IL-2 and IL-23 were maintained for all 14 days), and cultures were maintained at a maximum concentration of 2.0 × 10^6 cells/mL.

CD3-mediated redirected lysis of P815 cells

Isolated γδ T cells (effectors, 5.0 × 10^4) were added to a 96-well round-bottom tissue culture plate with P815 cells (targets, 1.0 × 10^4), and 0-5 μg/ml anti-CD3 (OKT3; Life Technologies). Each condition also included 5 μg/ml of either anti-NKG2A (Z199; Beckman Coulter) or mouse IgG_1 (MOPC-21). The effector and target cell cultures were centrifuged at 250 x *g* for 4 min prior to incubation at 37°C for 4 hr. The CytoTox 96® Non-Radioactive Cytotoxicity Assay kit (Promega) was then used to quantitate LDH release according to the manufacturer's instructions.

Briefly, plates were centrifuged at 250 x *g* for 4 min, and 50μl/well supernatant was transferred to a Nunc Maxisorp ELISA plate (Thermo Fisher). Fifty microliters of substrate solution was added to each well for 30 min before the addition of 50μl/well stop solution, and absorbance measured at 492nm. All samples were run in duplicate, and average absorbance values were used in cytotoxicity calculations. Maximum LDH release was determined by the addition of lysis solution to wells containing P815 cells only and spontaneous LDH release for each cell type calculated by incubation of P815 and γδ T cells alone. Background absorbance was determined from RF10 only controls and subtracted from all other absorbance readings. Percent cytotoxicity was calculated with the formula: [(experimental – effector spontaneous – target spontaneous)/(target maximum – target spontaneous)] × 100.

An aliquot of the isolated γδ T cells was also used to confirm the proportion of Vδ2$^+$ T cells among the effector population, as well as the proportion of cells with a CD94^{hi} phenotype, by flow cytometry.

QUANTIFICATION AND STATISTICAL ANALYSIS

Cells were acquired on a LSR Fortessa (BD Biosciences) and data analyzed using FlowJo v10.2 (TreeStar). In all experiments, lymphocytes were identified based on forward scatter (FSC) versus side scatter (SSC). Singlets were gated by FSC-A versus FSC-H, and live cells were identified by viability dye exclusion. A representative gating strategy for the identification of Vδ2$^+$, MR1 tet$^+$, conventional T cell and NK cell populations is shown in Figures S1A and S1B. Gates for phenotypic markers were determined based on fluorescent minus one (FMO) controls or, for bright and dim staining populations, bulk T cell or NK cell staining patterns. Quantification of Zeb2 mRNA expression by flow cytometry was performed using the PrimeFlow RNA assay (Thermo Fisher) according to the manufacturer's instructions. Pre-designed probes for Zeb2, RPL13A (positive control) and dapB (negative control) were used in all experiments. Gates for Zeb2-Alexa647 were set using the staining of dapB-Alexa647 as a control. In donors with low frequencies of Vδ2$^+$ T cells (particularly the HIV-infected cohorts), a minimum of 50 events was required for further phenotypic analysis of any given cell population. The only exception to this was the cord blood samples, where sample was limited.

RNaseq analysis was performed using the web-based Galaxy platform maintained by Melbourne Bioinformatics (Afgan et al., 2015). Reads were mapped to the *Homo sapiens* reference genome (hg19) using HISAT2 (Kim et al., 2015) and reads were quantified using HTSeq (Anders et al., 2015). Count matrices were generated and inputted into Degust (http://degust.erc.monash.edu) for data analysis and visualization. Heatmaps were generated using Morpheus (The Broad Institute; https://software.broadinstitute.org/morpheus/) and show the logFC for a given gene in the indicate group compared to the average expression level across all groups. Unless otherwise indicated, genes were considered to be differentially regulated if the false discovery rate (FDR) was < 0.05 and the absolute fold change (FC) was > 1.5. To generate a list of genes distinguishing MAIT and CD26^{hi}CD94^{lo} Vδ2$^+$ cells from both CD8$^+$ T cells and CD26$^{+/-}$ Vδ2 cell subsets, all genes that were differentially regulated between MAIT versus CD8$^+$ T cells, and

$CD26^{hi}CD94^{lo}$ versus the three other $V\delta2^{+}$ subsets were identified (FDR < 0.05, FC > 2). Genes appearing in both lists, with the same direction of regulation and with count per million values > 5 for at least one cell subset were selected. Heatmap shows the expression of each gene among the 6 cell subsets relative to the average. Clustering was performed using a hierarchical clustering algorithm.

TCR δ chain sequences were extracted from RNaseq datasets and assembled using MIXCR (Bolotin et al., 2015). Clonotypic relationships between γδ T cell subsets were established using VDJtools (Shugay et al., 2015) and visualized in R using circlize (Gu et al., 2014) and VennDiagram (Chen and Boutros, 2011) packages.

For all data other than the RNA sequencing data, statistical analysis was performed using Prism 7 (GraphPad). For analysis of two groups, Wilcoxon matched pairs test was employed. A Friedman test, followed by Dunn's post-test, was used in the analysis of more than two groups. For assessment of the interactions of two independent variables, a 2-way ANOVA was used. Correlations were performed using Spearman's test. A two-tailed P value less than 0.05 was considered significant. For each experiment, the figure legend indicates the number of donors used in the study (n), the number of replicates (where applicable) and the statistical test used for analysis.